The Radial Extent and Warp of the Ionized Galactic Disk. II. A Likelihood Analysis of Radio-Wave Scattering Toward the Anticenter

T. Joseph W. Lazio[1,2] & James M. Cordes
Department of Astronomy and National Astronomy & Ionosphere Center, Cornell University, Ithaca, NY 14853-6801;
lazio@spacenet.tn.cornell.edu, cordes@spacenet.tn.cornell.edu

ABSTRACT

We use radio-wave scattering data for extragalactic sources and pulsars to constrain the distribution of ionized gas in the outer Galaxy. Like previous models, our model for the H II disk includes parameters for the radial scale length and scale height of the ionized gas. In addition, we have used the known H I distribution in the outer Galaxy in constructing our model, and we allow the H II disk to warp and flare. We also include the Perseus arm in our model. We use a likelihood analysis on 18 anticenter sources with measured scattering observables: 11 extragalactic sources and 7 pulsars. We find that the strength of scattering in the Perseus arm is no more than 60% of the level contributed by spiral arms in the inner Galaxy and is equivalent to a scattering diameter of 1.5 mas at 1 GHz. Our analysis favors an unwarped, non-flaring disk with a scale height of 1 kpc, though this may reflect the non-uniform and coarse coverage of the anticenter provided by the available data. One extragalactic source has a size a factor of two smaller than predicted by our model, possibly indicating the existence of holes in the scattering material. The lack of a warp in the scattering material indicates that VLBI observations near 1 GHz with an orbiting station having baseline lengths of a few Earth diameters will not be affected by interstellar scattering at moderate Galactic latitudes, $|b| \approx 15°$. The radial scale length is 15–20 kpc, but the data cannot distinguish between a gradual decrease in the electron density and a truncated distribution. We favor a truncated one, because we associate the scattering with massive star formation, which is also truncated near 20 kpc. A radial extent of 20 kpc is also comparable to the radial extent of Hα emission observed for nearby spiral galaxies. We find that the distribution of electron density turbulence must decrease more rapidly with Galactocentric distance than the distribution of hydrogen. Alternate ionizing and turbulent agents—the intergalactic ionizing flux and the passage of satellite galaxies through the disk—are unlikely to contribute significant amounts to scattering in the anticenter. We cannot exclude the possibility that a largely

[1]NRC/NRL Post-doctoral Associate

[2]Current address: NRL, Code 7210, Washington, DC 20375-5351; lazio@rsd.nrl.navy.mil

ionized, but quiescent disk extends to $\gtrsim 100$ kpc, similar to that inferred for some Lyα absorbers.

Subject headings: Galaxy:structure — scattering — turbulence

1. Introduction

Early investigations of the Galaxy's H I emission revealed that it extends well past the solar circle, and that, in the outer Galaxy, the emission is warped systematically from its midplane in the inner Galaxy (Burke 1957; Kerr 1957; Westerhout 1957; Oort, Kerr, & Westerhout 1958). More recent stellar (Djorgovski & Sosin 1989), infrared (Sodroski et al. 1987; Freudenreich et al. 1994), and molecular (Wouterloot et al. 1990) observations have shown that these disk constituents also extend well past the solar circle and are warped similar to the H I layer.

Ionized gas occupies potentially 10% or more of the volume of the interstellar medium (ISM) near the solar circle and is probably a dynamically important constituent (e.g., Reynolds 1977; Kulkarni & Heiles 1987), but its radial extent is poorly constrained. Hα measurements are limited to distances of a few kiloparsecs by interstellar absorption (Reynolds 1983). The frequency at which the Galactic plane becomes optically thick because of free-free absorption can indicate the extent of the disk, but for plausible disk sizes (see below) this frequency is less than 10 MHz and so is difficult to observe. Few pulsars are known in the anticenter direction. Less than ten have dispersion-measure–independent distance estimates (DM $= \int n_{\rm e}\, ds$) and the estimated distances are less than 2 kpc (Frail & Weisberg 1990); the remainder have DMs of 30–125 pc cm^{-3}, consistent with distances of a few kiloparsecs (Taylor, Manchester, & Lyne 1993; Zepka et al. 1996). Fluctuations in the ionized gas produce radio-wave scattering which manifests itself as angular broadening of compact sources (see Rickett 1990 for a review of the full variety of interstellar radio wave propagation effects). Scattering measurements have been biased toward the inner Galaxy, even for surveys of angular broadening of extragalactic sources (e.g., Fey, Spangler, & Mutel 1989; Fey, Spangler, & Cordes 1991). Only one angular broadening survey has been conducted toward the outer Galaxy (Dennison et al. 1984), and, as we illustrate below, most of the sources in that survey had Galactic latitudes too large to provide effective constraints on the radial extent of the ionized Galactic disk. Measurements of interplanetary scintillation determine source diameters indirectly, but in general do not have sufficient resolution to provide stringent constraints.

Though the radial extent of the ionized gas is poorly constrained, a number of lines of evidence suggest that its radial extent may equal or exceed that of the H I:

- Savage, Sembach, & Lu (1995) find C IV absorption along the line of sight to H 1821+643 ($\ell = 94°, b = 27°$). Among the velocity components contributing to this absorption is low-density ($n \sim 5.6 \times 10^{-3}$ cm^{-3}), warm ($T \sim 10^4$ K) gas at a velocity of -120 km s^{-1}, corresponding to a kinematic Galactocentric distance of 25 kpc.

- The H I disks of nearby galaxies are truncated at radii of order 25–50 kpc, at which the surface density drops to $N_{\rm H\,I} \lesssim 2 \times 10^{19}$ cm^{-2} (Corbelli, Schneider, & Salpeter 1989; van Gorkom 1991; Bland-Hawthorn 1997). This truncation is observed even for galaxies without nearby companions and likely occurs where the disks become optically thin to the intergalactic ionizing flux (Sunyaev 1969; Corbelli & Salpeter 1993). Bland-Hawthorn, Freeman, & Quinn (1997) have reported the detection of ionized gas beyond the observed H I disk of NGC 253. Charlton, Salpeter, & Hogan (1992) have proposed that at least some of the low-redshift Lyα clouds seen in quasar spectra may be due to residual H I in extended, nearly fully ionized disks of normal spiral galaxies. Our Galaxy would then be a prototypical, $z = 0$ absorber.

- Material blown out of the Galactic disk by the action of clustered supernovae may account for a fraction of high-velocity clouds and later return to the disk forming a Galactic fountain (Shapiro & Field 1976; Bregman 1980; Houck & Bregman 1990; Spitzer 1990; Kahn 1991). Models of high-velocity clouds often require the material to be supported by gas pressure at large Galactocentric radii, $R \gtrsim 25$ kpc (e.g., Bregman 1980).

Taylor & Cordes (1993, hereinafter TC93) modelled the Galactic distribution of ionized gas with three global components:

1. an extended component with scale height of approximately 1 kpc and $1/e$ radial scale length of order 20 kpc;

2. an inner Galaxy component with scale height of 0.15 kpc and radial scale length of 3.5 kpc; and

3. spiral arms, the number and shape of which were determined by appeal to radio and optical observations of H II regions and radio observations of H I and non-thermal emission.

The data available to constrain the model parameters consisted of 74 pulsars with DM-independent distances, 223 scattering measurements toward pulsars, masers, and extragalactic sources, and the Galactic longitude distribution for 553 pulsar DMs.

Because of the paucity of measurements summarized above, TC93 could place only a lower bound on the scale length of the extended component, A_1. They adopted $A_1 = 20$ kpc, though $A_1 \approx 50$ kpc produced comparable fits to the data. Moreover, they modelled the extended component as planar; if the ionized disk does extend to 20 kpc or more, it is likely to be warped similarly to the other outer Galaxy disk constituents.

Figure 1 demonstrates that angular broadening measurements of extremely low-latitude, $|b| < 1^\circ$, extragalactic sources toward the Galactic anticenter have the potential of constraining A_1. The line of nodes of the H I disk is fairly constant with Galactocentric radius and is near a Galactic longitude of 170°, so sources toward the anticenter probably provide the longest path length

through the ionized disk. Extremely low-latitude sources are required because the scale height of the extended component near the solar circle is 0.88 kpc and only for sources with $|b| < 1^\circ$ does the line of sight remain within one scale height for path lengths of 50 kpc or more. Only three of the sources in Dennison et al.'s (1984) survey meet this criterion; of these, one may show excessive scattering due to an H II region along the line of sight and another shows complex structure making it difficult to estimate a scattering diameter.

We have carried out a program of multifrequency Very Long Baseline Array (VLBA) observations of twelve anticenter sources, seven of which have $|b| < 0.^\circ 5$ (Lazio & Cordes 1997, hereinafter Paper I). We detected all but one of the sources at one or more of our observation frequencies—0.3, 1.6, and 5 GHz. As Fig. 1 illustrates, the nominal resolutions of the VLBA are such that 18 cm observations are sensitive to scale lengths of $A_1 \gtrsim 100$ kpc and 90 cm observations should detect scattering even if $A_1 \lesssim 10$ kpc.

Figure 1 also shows the nominal resolution of the space VLBI satellite HALCA, and thereby illustrates another important aspect of improving our knowledge of the Galactic distribution of scattering. At low Galactic latitudes, interstellar scattering will determine the limiting resolution for baselines in excess of the Earth's diameter at frequencies near 1 GHz. If the H II disk flares or warps similarly to the H I disk, interstellar angular broadening could be non-negligible at much higher latitudes (e.g., $|b| \approx 30^\circ$).

In this paper we combine the sources from our survey with other radio-wave scattering measurements from the literature and use a likelihood analysis to constrain the distribution of ionized gas in the outer Galaxy. In §2 we describe our model for the distribution of ionized gas in the outer Galaxy, in §3 we extract scattering diameters from our measured angular diameters and develop a likelihood analysis of scattering in the outer Galaxy, and in §4 we discuss our results and present our conclusions.

2. A Model of the Ionized Disk in the Outer Galaxy

In this section we develop a model for the distribution of free electrons in the outer Galaxy. Based on the close correspondence between the H I disk and other outer Galaxy constituents, §1, we shall use the H I distribution in the outer Galaxy as a basis for modifying the TC93 model. We begin with a discussion of the connection between the observed scattering angle, $\theta_{\rm s}$, and the (modelled) electron density, $n_{\rm e}$.

2.1. Electron Density Fluctuations and Angular Broadening

The density fluctuations responsible for angular broadening are parameterized commonly with a power-law spectrum,

$$P_{\delta n} = C_n^2 q^{-\alpha}, \tag{1}$$

over a range of spatial wavenumbers, $q_0 \ll q \ll q_1$, where $l_0 = 2\pi/q_0$ and $l_1 = 2\pi/q_1$ are the outer and inner scales, respectively, to the spectrum. The quantity C_n^2 sets the amplitude of the density fluctuations and varies spatially. Throughout we adopt a spectral index of $\alpha = 11/3$, the Kolmogorov value, as suggested by a number of observations (Rickett 1990).

The scattering angle for plane-wave radiation propagating a distance D through a medium filled with such a spectrum of density fluctuations is (Cordes et al. 1991; Cordes & Lazio 1991)

$$\theta_{\rm s} = 128\,{\rm mas}\,{\rm SM}^{3/5}\nu_{\rm GHz}^{-11/5}. \tag{2}$$

The quantity SM is the line-of-sight integral of C_n^2,

$${\rm SM} = \int_0^D ds\, C_n^2(s), \tag{3}$$

and $\nu_{\rm GHz}$ is the frequency in GHz.

Cordes et al. (1991) demonstrated that the level of scattering, as measured by SM, correlates with the dispersion measure, DM, for nearby pulsars; for pulsars toward the inner Galaxy, the level of scattering increases faster with distance than DM. This correlation suggests that the electrons responsible for dispersion are also responsible for scattering. Cordes et al. (1991) and TC93 adopted

$$d{\rm SM} = C_{\rm u} F n_{\rm e}^2\, ds. \tag{4}$$

Here $n_{\rm e}$ is the electron density in cm^{-3}, F is the fluctuation parameter and is a measure of how effectively density fluctuations are produced and maintained, ds is a path length interval in kpc, and $C_{\rm u}$ is a constant responsible for producing SM in the typical units of kpc m$^{-20/3}$, $C_{\rm u} = 3.4(2\pi)^{-1/3}$ m$^{-20/3}$ cm^6. With a model for $n_{\rm e}$ in the outer Galaxy, we can integrate equation (4) along the line of sight to a source to find SM and $\theta_{\rm s}$.

2.2. Free Electron Density Model

Of the four components in the TC93 model, only the spiral arms and the extended component are relevant to our study of the outer Galaxy. The inner Galaxy component has a scale length of 3.5 kpc and, at the solar circle, its contribution to the electron density has decreased to 0.2% of that from the extended component. The Gum Nebula, which was also included in the model because of its proximity to the Sun, only affects lines of sight within about 20° of $(\ell, b) = (260°, 0°)$, well removed from the directions to the sources considered here.

We retain the spiral arm component because one of the spiral arms, the Perseus arm, is outside the solar circle over the longitude range of interest. Lines of sight with $|b| \lesssim 10^\circ$ pass within one scale height of the center of this spiral arm. In the TC93 model, this arm contributes a scattering measure of SM ~ 0.01 kpc m$^{-20/3}$, equivalent to a 1 GHz scattering angle of $\theta_{\rm s} \sim 10$ mas for the line of sight $(\ell, b) = (180^\circ, 0^\circ)$.

The remaining component is the extended component. In the TC93 model this component consisted of a flat disk, centered on the Galaxy's midplane with a scale height $h_1 = 0.88$ kpc and scale length $A_1 = 20$ kpc. We use H I observations toward the outer Galaxy as a guide for constructing our model for three reasons. First, in the inner Galaxy, the mean and rms electron density distributions generally follow the distribution of massive stars, and, toward the outer Galaxy, sites of massive star formation follow the H I distribution (Wouterloot et al. 1990). Second, Savage et al. (1995) detected ionized gas that is spatially coincident with warped H I gas. Finally, models of low-redshift Lyα clouds, in which the outer extent of the Galaxy is nearly fully ionized by the intergalactic ionizing flux (Charlton et al. 1993), predict that the H I disk is ionized to form the H II disk. The H I structure in the outer disk has been reviewed by Burton (1992). Here we shall only summarize salient details as we construct our model for the outer H II disk.

In the outer Galaxy the distribution of $n_{\rm e}$ is the sum of the extended component and the Perseus arm,

$$n_{\rm e}(x, y, z) = n_1 g_1(R) \, {\rm sech}^2[Z(R)/h_1(R)] + f_4 n_{\rm a} \, {\rm sech}^2(z/h_{\rm a}) g_{\rm a}(R, d). \tag{5}$$

The nominal densities of the two components are $n_{1,{\rm a}}$; their radial dependences are given by the functions $g_{1,{\rm a}}$; and their scale heights by $h_{1,{\rm a}}$, respectively. The midplane of the extended component is given by $Z(R)$ and the Perseus arm has a fine-tuning parameter of f_4. The following sections explain the various quantities in more detail. As in TC93 the coordinate system has the x-axis directed parallel to $\ell = 90^\circ$, the y-axis directed parallel to $\ell = 180^\circ$, the z-axis directed toward $b > 0^\circ$, and the Galactocentric radius is $R = \sqrt{x^2 + y^2}$. The minimum distance between the position (x, y) and a point on the Perseus arm is denoted by d (see TC93 for a full description of the spiral arms). Following TC93 we take the radial and z dependences to be separable.

2.2.1. Radial Dependence of the Extended Component

We consider two functional forms for the radial dependence of the extended component, $g_1(R)$. The first is a sech^2 dependence

$$g_1^{(1)}(R) = {\rm sech}^2 \left(R/A_1^{(1)} \right) / {\rm sech}^2 \left(8.5\,{\rm kpc}/A_1^{(1)} \right). \tag{6}$$

We shall refer to this as a sech^2 disk. This functional form exhibits a gradual decrease in the electron density with R; for $R \gg A_1^{(1)}$, $g_1^{(1)}(R) \propto \exp\left(-2R/A_1^{(1)}\right)$. The second form is

$$g_1^{(2)}(R) = \begin{cases} \cos\left(\pi R/2A_1^{(2)}\right) / \cos\left(\pi R_\odot/2A_1^{(2)}\right), & R \le A_1^{(2)}; \\ 0, & R > A_1^{(2)}. \end{cases} \tag{7}$$

We shall refer to this as a truncated disk because it is zero for $R > A_1^{(2)}$.

Figure 2 compares these functional forms with each other and with the H I density (Gordon & Burton 1976). Our choice for these particular functional forms is motivated by a number of considerations: The sech^2 dependence is that assumed by TC93 and so our results can be compared directly to theirs. When compared to the H I density, the sech^2 disk has a slower radial fall off while the truncated disk has a faster radial fall off. These two functional forms should bracket the actual A_1 if the electron density distribution follows that of the H I. The truncated disk also allows us to model a disk with variable scattering properties. At $R > A_1^{(2)}$ there is no additional scattering. As we have written equation (7), this truncation occurs because $n_\mathrm{e} = 0$ cm^{-3} for $R > A_1^{(2)}$. An equivalent model is one in which there is ionized gas but $F_1 = 0$ for $R > A_1^{(2)}$. Such a truncation could occur if the distribution of scattering agents decreased more rapidly with R than does n_e. Finally, our estimates of A_1 are model dependent. Comparison of the two forms allows us to assess the sensitivity of our estimates of A_1 to the assumed models. Both functions are normalized so that $g_1(R_\odot) = 1$. Henceforth, we shall drop the superscripts (1) and (2) as it will be clear from the context which A_1 parameter we are describing.

2.2.2. z-dependence of the Extended Component and the Galactic Warp

The z-dependence of the outer Galaxy density distribution is allowed to differ from that of the TC93 model by two effects. First, the H I disk is observed to flare to larger scale heights as R increases. We model this effect by allowing the scale height to vary with Galactocentric distance, $h_1(R)$. The second is that the H I layer is warped. The actual shape of the H I warp is complex, with differences between the northern and southern Galactic hemispheres and with an amplitude that is radially dependent (though other tracers of the outer disk are more symmetric than the H I, Djorgovski & Sosin 1989; Wouterloot et al. 1990). Because the longitude range of our data, $150^\circ < \ell < 210^\circ$, is significantly less than the 180° longitude range over which the north/south asymmetry is important, we shall ignore the asymmetry in the warp.

The scattering measure is an integrated quantity, while H I and CO measurements yield velocity information. We therefore model the outer ionized disk as a single tilted ring or torus. Our approximation to the disk in the outer Galaxy is illustrated in Fig. 4.

The H I disk begins to warp and flare significantly at the same radius, $R \approx 10.5$ kpc. The line of nodes of the H I disk varies with R, but is approximately centered on $\ell = 170^\circ$. The onset of

the H II warp is assumed to occur at the same radius as the H I warp does. At $R < 10.5$ kpc, our model agrees with the TC93 model, with a scale height, $h_{1,\rm in}$, and fluctuation parameter, $F_{1,\rm in}$. At $R > 10.5$ kpc the H II disk is tilted by an angle Ψ with respect to $b = 0°$, has a line of nodes ℓ'_0, a scale height $h_{1,\rm out}$, and fluctuation parameter $F_{1,\rm out}$. The radial dependences in equations (6) and (7) are continuous through $R = 10.5$ kpc.

In the warped disk, the z-dependence and scale height in equation (5) are relative to the midplane of the gas, *not* to $b = 0°$, cf. Fig. 4. Interior to the warp, the distance above the plane is $Z = s \sin b$ where s is a distance along the line of sight. Within the warp a source with with Galactic coordinates (ℓ, b) has a latitude b' relative to the torus' midplane. The corresponding z-height is $Z = s \sin b'$ where b' is given by

$$\sin b' = \sin b \cos \Psi + \cos b \sin(\ell - \ell'_0) \sin \Psi. \tag{8}$$

The warped portion of the disk is assumed axisymmetric, as is the unwarped extended component.

The division between $F_{1,\rm in}$ and $F_{1,\rm out}$ is to allow for the possibility that the mechanism for generating or maintaining density fluctuations in the far outer Galaxy may differ from that in the inner Galaxy. The radius at which the transition from $F_{1,\rm in}$ to $F_{1,\rm out}$ occurs was chosen to be that at which the disk begins to flare and warp significantly. The key assumption utilized here is that the flaring and warping may be symptomatic of other processes which could result in a change $F_{1,\rm in}$ to $F_{1,\rm out}$.

2.2.3. Spiral Arm Component

The functional dependences for the spiral arm component are unaltered from the TC93 model. In particular, the radial dependence for the spiral arms is

$$g_{\rm a}(R, d) = \begin{cases} \exp[-(d/w_{\rm a})^2], & R \le A_{\rm a}, \\ \exp[-(d/w_{\rm a})^2] \, \mathrm{sech}^2[(R - A_{\rm a})/2], & R > A_{\rm a}, \end{cases} \tag{9}$$

with $A_{\rm a} = 8.5$ kpc a scale length analogous to A_1 and $w_{\rm a} = 0.3$ kpc the width of a spiral arm.

2.3. Preliminary Constraints on Model Parameters

The source 87GB 0558+2325 has a measured diameter of approximately 4 mas at 1 GHz (Paper I), a factor of two less than that predicted by the Perseus arm's contribution alone (TC93). In order that our model not overpredict scattering diameters, we must modify the spiral arm component as well. Of the nine parameters[3] describing the spiral arms—$n_{\rm a}$, $h_{\rm a}$, $F_{\rm a}$, $w_{\rm a}$, $A_{\rm a}$, and

[3] Strictly speaking, the shapes of the arms are described by fiducial points which are also parameters. However, they have been determined largely from radio and optical observations of H II regions and radio observations of thermal and H I emission. We have not altered the fiducial points.

four fine-tuning parameters, f_j—TC93 used DM and scattering data to fit for the first three. They appealed to other radio and optical observations in fixing $w_{\rm a} = 0.3$ kpc and $A_{\rm a} = 8.5$ kpc. In the inner Galaxy TC93 used the f_j to obtain better agreement between the model and observations toward the tangent points of certain spiral arms. In the TC93 model f_4, the fine-tuning parameter for the Perseus arm, was set to unity; we shall allow it to vary.

Our justification for allowing only f_4 to vary is that it is the only spiral arm parameter that can be modified without affecting the model in the inner Galaxy. While the nine sources from our survey in Paper I are a substantial fraction of the number of available scattering measurements toward the anticenter, cf. Table 2 and Fig. 3, the total number of scattering measurements toward the anticenter is only approximately twenty. This number is a small fraction of the nearly 300 DM and SM measurements that TC93 used to constrain the model parameters. Thus, incorporating our additional measurements from Paper I into the 300 used by TC93 and repeating their analysis would not lead to any substantial change of the model in the inner Galaxy.

With the above model we can now integrate dSM, equation (4), along the line of sight toward a source at (ℓ, b) to form SM. Since the two components have unequal fluctuation parameters, the contribution from each component is determined separately, then summed to form the total scattering measure. The predicted angular diameter is given by equation (2) where the modelled SM is a function with the following parameters $\widehat{\rm SM} = \widehat{\rm SM}(n_1, f_4, A_1, h_{1,\rm in}, h_{1,\rm out}, F_{1,\rm in}, F_{1,\rm out}, \ell_0', \Psi|\ell, b; R_{\rm warp})$.

3. Analysis

In this section we describe how we have used the measured angular diameters (Paper I) to obtain scattering diameters, discuss additional scattering measurements we have used in our analysis, develop the likelihood functions we will use to constrain the model parameters, and present the results of this likelihood analysis.

3.1. Determination of Scattering Diameters

For each source we have a measurement of its apparent angular diameter at one to three frequencies, $\theta_{\rm app}(\nu)$. We assume the apparent diameter is a quadrature sum of the intrinsic and scattering diameters and model it as

$$\theta^2_{\rm app}(\nu) = \frac{\theta^2_{\rm i}}{\nu^{2\alpha}} + \frac{\theta^2_{\rm s}}{\nu^{4.4}}. \tag{10}$$

Here $\theta_{\rm i}$ and $\theta_{\rm s}$ are the intrinsic and scattering diameters at 1 GHz, respectively. For the scattering diameter we have used the $\nu^{-2.2}$ dependence, as is appropriate for moderately strong scattering. For a homogeneous source with a peak brightness temperature T_B, $\alpha = 1$ (Kellermann & Owen 1988).

We have considered a number of ways of using equation (10) to solve for θ_s.

1. Ignore intrinsic size: Setting $\theta_i = 0$ mas, $\theta_s = \theta_{app}\,\nu_{GHz}^{2.2}$. Since this method assumes that scattering dominates the apparent diameter, the scattering diameter so derived is an upper limit.

2. Dual frequency measurements: For sources with angular diameters measured at 18 and 90 cm, if we set $\alpha = 1$, we have two equations in two unknowns and can solve for θ_i and θ_s.

3. Ignore scattering at high frequencies and assume homogeneous sources: At 6 cm, scattering should be unimportant for lines of sight to the outer Galaxy. For those sources detected at 6 cm, we take the 6 cm diameter to be the intrinsic diameter and scale it to 1 GHz, with $\alpha = 1$. We use the *observed* frequency dependence to find the 1 GHz apparent diameter from the 18 and 90 cm diameters. The scattering diameter is then found by subtracting in quadrature the scaled intrinsic diameter from the apparent diameter.

4. Ignore scattering at high frequencies: The final method also utilizes 6 cm diameters. Rather than assuming $\alpha = 1$ in scaling the intrinsic diameter to 1 GHz, we solve for α using the 6 and 18 cm diameters, assuming $\theta_s = 0$ mas. Then, using the 18 and 90 cm diameters to solve for the 1 GHz apparent diameter, we again subtract in quadrature the scaled intrinsic diameter from the apparent diameter.

Clearly not all of these methods can be used for all sources. For those sources for which multiple methods can be used, we utilize as many of the methods as possible and then adopt the estimate which places the most stringent limit on θ_s. In general, method 2 and method 1 produce estimates of θ_s that are the same within the errors. We note that using method 1 tends to bias us toward larger disk scale lengths because this method assumes that the intrinsic size makes no contribution to the measured diameter. We find 1 GHz scattering diameters or limits in the range 1.5–48 mas; these are tabulated in Table 1.

3.2. Available Data

We augment the scattering measurements from our survey (Paper I) with others from the literature within the same longitude range, $150° \leq \ell \leq 210°$. These are summarized in Table 2, scaled to 1 GHz. Two kinds of scattering measurements were found in the literature: angular broadening measurements similar to those reported here and scintillation bandwidth, $\Delta\nu_d$, measurements of pulsars (Cordes 1986).

The resulting data set consists of three classes of sources having the following observables:

1. Extragalactic sources having measured scattering diameters or upper limits on the scattering diameter, θ_s; 11 such sources;

2. Pulsars with DM-independent distance estimates. This class has only one member, the Crab pulsar, for which a DM and scattering diameter have been measured.

3. Pulsars without DM-independent distance estimates; 10 such sources with measured DM and $\Delta\nu_{\rm d}$.

All of these sources are shown in Fig. 3.

Two of the pulsars that have a measured scintillation bandwidth will not be included in our analysis. The lines of sight to the pulsars PSR B0823+26 and PSR B1112+50 are likely to be dominated by local scattering material. Both pulsars are closer than 0.5 kpc, closer than the inner edge of the Perseus arm.

Our intention is to constrain the distribution of scattering material in the outer Galaxy. In selecting extragalactic sources to include in our analysis, we have focussed on sources for which scattering makes a measurable contribution the observed diameter. Such sources are marked by visibility functions displaying a gaussian-like profile with increasing baseline length or by images containing only simple structures, typically a single gaussian component. An alternate approach would be include in our analysis *all* extragalactic sources in the anticenter. Since the observed angular size is a convolution of the intrinsic size with the scattering diameter, we can always derive an upper limit to the scattering diameter for any source (see Method 1 in §3.1). However, these upper limits are usually factors of at least 5–10 larger than the scattering diameters predicted by the TC93 model. Sources for which scattering appears to dominate the observed angular diameters suggest that the level of scattering toward the anticenter is actually less than that predicted by the TC93 model. The upper limits for the scattering diameters of most sources therefore place no meaningful constraint on the scattering toward the anticenter (see also §3.5). We illustrate the lack of constraints provided by most sources with four sources originally included in the TC93 analysis, but not included in this analysis.

Four extragalactic sources included in the TC93 analysis are not included here, because a re-analysis of the existing observations suggests that no scattering diameter has been measured. The four sources are CTA21 (0316+162), 0611+131, 4C14.18 (0622+147), and 3C190 (0758+143). In the TC93 analysis CTA21 and 3C190 were taken to have scattering diameters of approximately 200 mas at 74 MHz, based on a single-baseline VLBI experiment (Resch 1974). A later multi-station VLBI experiment at 609 MHz showed CTA21 to have a core-halo structure, with the halo having a size $\theta \geq 130$ mas (Wilkinson et al. 1979). Wilkinson et al. (1979) suggest that the halo is responsible for the interplanetary scintillation this source exhibits at 81 MHz. The halo is also likely to be the component responsible for the aforementioned 74 MHz angular diameter. The core itself appears to be a blend of two components. A characteristic size of these blended components is about 10 mas, equivalent to an upper limit on the scattering diameter of 3.4 mas at 1 GHz; this upper limit is more than a factor of 5 larger than the predicted TC93 scattering diameter. For 3C190, a later multi-station VLBI experiment at 609 MHz showed it to have three components of comparable flux and similar, steep spectra with diameters of approximately 100 mas (Rendong et

al. 1991). It is not clear if one of these components dominates at 74 MHz, and hence is responsible for the aforementioned angular diameter measurement, or if Resch's (1974) observations sample a complex visibility function and his results do not represent an actual diameter at all. The equivalent upper limit on the 1 GHz scattering diameter is approximately 40 mas, nearly a factor of 100 larger than the predicted model diameter. The source 4C14.18 has a steep spectrum and a non-gaussian visibility function (Dennison et al. 1984). By fitting a gaussian to the visibility data, they place an upper limit on the 1 GHz scattering diameter of 22 mas, more than a factor of 5 larger than that predicted by the TC93 model. The source 0611+131 was taken to have a scattering diameter of 40 mas at 408 MHz (Dennison et al. 1984) in the TC93 analysis. Our new observations at 1.6 and 5 GHz show this diameter to result from the blending of at least two source components (Paper I). We place an upper limit on the 1 GHz scattering diameter of 30 mas, a factor of 10 larger than the predicted value.

Our initial attempts to form the likelihood function included the Crab pulsar (PSR B0531+21). However, we found that it ended up dominating the resulting likelihood functions, in some cases contributing as much as 50% of the log-likelihood. Because the Crab is relatively nearby ($D \approx 2$ kpc), we do not believe it should be the dominant source in the likelihood function. The results presented here do not include the Crab.

The reason for the Crab's large contribution to the likelihood is a large discrepancy between the observed and modelled quantities: The observable quantities are DM = 56.8 pc cm^{-3} and $\theta_{\rm s} = 0.5 \pm 0.05$ mas, while typical values for these quantities in our models are $\widehat{\rm DM} \approx 30$ pc cm^{-3} and $\hat{\theta}_{\rm s} \approx 0.7$ mas. Our modelled values are comparable to those in the TC93 model. The models overpredict the scattering angle, while underpredicting the DM. In particular, the discrepancy in the observed *vs.* modelled DM results in a significant contribution to the likelihood function.

The Crab nebula is unlikely to be the source of the discrepancies. Its contribution to the DM is probably no more than 1% (Isaacman 1977). Its contribution to the scattering diameter is de-leveraged by a factor of order $L/D \sim 10^{-3}$ where L is the diameter of the nebula. Evidence supporting a small nebular contribution to the scattering diameter comes from comparing the measured scattering diameter with that inferred from pulse broadening for the pulsar. The pulse broadening has a variable and a constant component; the constant contribution arises from the ISM distributed between the pulsar and the Earth. The scattering diameter estimated from the constant pulse broadening agrees well with the observed scattering diameter (Vandenberg 1976; Isaacman & Rankin 1977; Gwinn, Bartel, & Cordes 1993). We conclude that the ionized gas along the line of sight to the Crab has a relatively high electron density but is not strongly turbulent.

We are left with a total of 18 sources, 11 extragalactic and 7 pulsars.

3.3. Likelihood Functions for Scattering in the Outer Galaxy

We shall use a likelihood analysis to constrain the parameters of the ionized disk model presented in §2.2.

For the $i^{\rm th}$ line of sight, the probability of obtaining the observable x ($\theta_{\rm s}$, DM, or $\Delta\nu_{\rm d}$) is

$$\begin{aligned} p\left(x_i|\hat{x}_i\right) &\approx f_x\left(x_i|\hat{x}_i\right)\delta x_i \\ &= \frac{1}{\sqrt{2\pi}}\exp\left[-\frac{1}{2}\left(\frac{x_i-\hat{x}_i}{\delta x_i}\right)^2\right]. \end{aligned} \tag{11}$$

where $\hat{x}_i$ is the value predicted for that line of sight and δx_i is the uncertainty associated with the measured value of the observable. For many of the extragalactic sources we have only an upper limit to a scattering diameter, because the scattering diameter has been estimated from a single frequency. The probability that a scattering observable x is less than an upper limit X is

$$\begin{aligned} p\left(x_i \le X_i|\hat{x}_i\right) &= \int_0^{X_i} dx'\, f_x\left(x'|\hat{x}_i\right) \\ &= \frac{1}{2}\left[\mathrm{erf}\left(\frac{X_i-\hat{x}_i}{\delta x_i\sqrt{2}}\right)+\mathrm{erf}\left(\frac{\hat{x}_i}{\delta x_i\sqrt{2}}\right)\right] \end{aligned} \tag{12}$$

where $\mathrm{erf}(x)$ is the error function.

The global likelihood function for all sources is

$$P = \prod_{i=1}^{N} p_i. \tag{13}$$

The modelled quantities and measurement uncertainties for the various classes of sources are as follow:

1. The predicted extragalactic scattering diameters are found by integrating dSM along the line of sight and using equation (4). Most of the extragalactic source scattering diameters in the literature are single frequency measurements; we scale the errors for these to 1 GHz assuming a $\lambda^{2.2}$ dependence. For the scattering diameters we report, the errors are estimated from the formal statistical errors on the fits to the data and then scaled (single-frequency measurement) or propagated (multiple-frequency determination) to 1 GHz. The uncertainties are 10–25%.

2. For the pulsars we integrate $n_{\rm e}\,ds$ and a weighted form of equation (4) until the modelled DM equals the measured DM. The appropriate weighting factor for the scintillation bandwidth is $w(s) = (s/D)(D-s)/D$, where D is the distance to the source and s is the distance along the line of sight. This weighting factor accounts for the fact that $\Delta\nu_{\rm d}$ is a measure of

the excess time delay taken by scattered lines of sight. The scintillation bandwidth is then calculated as

$$\Delta\nu_{\rm d} = 145\,{\rm Hz}\,D_{\rm kpc}^{-1}({\rm SM})^{-6/5}, \tag{14}$$

with SM in the conventional units of kpc m$^{-20/3}$ and $D_{\rm kpc}$ the distance in kpc. The measurement uncertainties for $\Delta\nu_{\rm d}$ range from 20% to 70%; we adopt $\delta(\Delta\nu_{\rm d})/\Delta\nu_{\rm d} = 0.33$.

3.4. Results

We have searched for the maximum of the global likelihood, equation (13), using an iterative grid search procedure. Initial ranges for the various parameters, described in more detail below, were estimated based on the TC93 model results and the structure of the H I disk. Then the ranges and the grid search resolutions were refined to locate the maximum.

The model in §2.2 contains nine parameters: f_4, n_1, A_1, $h_{1,\rm in}$, $h_{1,\rm out}$, $F_{1,\rm in}$, $F_{1,\rm out}$, ℓ_0', and Ψ. We held n_1 and $h_{1,\rm in}$ fixed at their values in the TC93 model, $n_1 h_{1,\rm in} = 0.0165$ kpc cm^{-3} and $h_{1,\rm in} = 0.88$ kpc ($n_1 = 0.0188$ cm^{-3}). These quantities are constrained by the DMs of high-latitude pulsars, particularly those in globular clusters. There is only one high-latitude pulsar, B0301+19 ($b = -33°$) in our sample, and it is not in a globular cluster. Further, n_1 and $h_{1,\rm in}$ describe the ionized medium near the solar circle and were constrained (along with nine other parameters) by a fit to nearly 300 DM and SM measurements. As we discuss at the end of §2.2, we do not expect our more limited set of measurements to change appreciably those parameters which describe the electron density distribution in the inner Galaxy or even near the solar circle.

We show that $F_{1,\rm in}$ may have a value different than that adopted in the TC93 model. Because $F_{1,\rm in}$ also affects sources in the solar neighborhood that we do not include in our data sample, we shall not conduct a grid search over it, but illustrate its effects by adopting one of two fiducial values.

The existence and amplitude of the warp are modelled by Ψ and ℓ_0'. From Fig. 3 it is apparent that the current complement of anticenter scattering measurements sample the outer Galaxy both coarsely and far from uniformly. In particular the sources are in three groups, with $\ell \approx 160°$, 180°–190°, and 200°. The number of sources (≈ 20) available for constraining the shape of the outer H II disk is also far smaller than the number used to describe the H I warp ($\sim 40\,000$ telescope beams, Burton & te Lintel Hekkert 1986), the H_2 warp (~ 1300 IRAS sources, Wouterloot et al. 1990), or the stellar warp ($\sim 20\,000$–$90\,000$ stars, Djorgovski & Sosin 1989; Carney & Seitzer 1993). Our survey is more restricted in longitude than these other surveys, but, even so, the above surveys have 10–100 times as many lines of sight. We shall therefore not conduct a search over Ψ or ℓ_0' but shall choose two fiducial pairs and compare the resulting maximum likelihood values. One pair will be for an unwarped disk, $\Psi = 0°$ (ℓ_0' is, of course, undefined for an unwarped disk), and the second pair will be characteristic of the warp in the H I disk, $(\Psi, \ell_0') = (20°, 170°)$.

In summary, we never attempted to fit for more than three parameters, A_1, $h_{1,\rm out}$, and $F_{1,\rm out}$ at a time. In the rest of this section, we place preliminary constraints on A_1, assess the importance of the Perseus arm, then reevaluate our constraints on A_1.

3.4.1. Preliminary Constraints on A_1

Figure 5 shows the likelihood as a function of A_1 for a model with an unwarped, non-flaring disk and in which the Perseus arm does not contribute to the scattering, i.e., $f_4 = 0$.

We have excluded PSR B0611+22 and the extragalactic source 0629+109 from this fit. The pulsar we exclude because its DM and scintillation bandwidth are likely to be affected by the Strömgren spheres of stars in the I Gem association (Weisberg, Rankin, & Boriakoff 1980). The extragalactic source we exclude because it has a 1 GHz diameter of 25 mas (Dennison et al. 1984), approximately a factor of five larger than that for extragalactic sources within a few degrees. The line of sight for this source passes close to the edge of the H II region Sharpless 273, $(\ell, b) \approx (202^\circ, 2^\circ)$. This H II region probably enhances the scattering for this line of sight. We retain these sources in the fits which include the spiral arm component (below) because the spiral arms have been incorporated in the TC93 model specifically to account for enhanced dispersion and scattering such as would occur from OB associations and H II regions.

The maximum likelihood occurs at $A_1 \approx 17$ kpc for a sech^2 disk while $A_1 \approx 25$ kpc for a truncated disk. The truncated disk is larger because there is no scattering material outside A_1 while, for the sech^2 dependence, A_1 is approximately the half-power point and there is a non-negligible amount of ionized gas at $2A_1$ ($\approx 10\%$). The likelihood favors the sech^2 disk, but by a factor less than two.

Provided that $F_{1,\rm out}$ is not substantially smaller than $F_{1,\rm in}$, these likelihood results place an upper limit on A_1. Any scattering contributed by the Perseus arm would reduce the estimate of A_1 (as the second panel of Fig. 5 illustrates and we discuss below). Similarly, allowing the disk to flare or warp or both produces, on average, larger scattering diameters for high-latitude sources. To reproduce a given scattering diameter in the absence of flaring or warping, the scattering material must extend to a large enough distance, i.e., A_1 must be large enough, to compensate for the z-dependent fall-off of the scattering material. As we demonstrate below, however, if $F_{1,\rm out}$ is quite small, as compared to $F_{1,\rm in}$, a much larger radial extent would be favored.

On the basis of Fig. 5, we conclude that the large A_1 values that were allowed by the TC93 analysis, e.g., $A_1 \approx 50$ kpc, are now shown to be disfavored.

3.4.2. Scattering in the Perseus Arm

The nominal Perseus arm in the TC93 model contributes enough scattering that some scattering diameters are overpredicted by a factor of two. Thus, we must decrease the amount of scattering contributed by this arm.

In the TC93 model this arm has a fluctuation parameter equal to that of all other arms, $F_{\rm a} = 6$, and a fine-tuning parameter $f_4 = 1$. Our model allows f_4 to vary. Since the Perseus arm scattering measure is SM $\propto F_{\rm a} f_4^2$, adjusting f_4 is equivalent to allowing the various arms to have different fluctuation parameters.

If we set $n_1 = 0$ cm^{-3}, thereby "turning off" the scattering in the disk, we determine how large f_4 must be to account for all of the scattering required by the observed scattering diameters. We have performed two separate fits for f_4, one using all of the sources, the second using just the extragalactic sources. Since the extragalactic sources are clearly well beyond all of the Galaxy's scattering material, the extragalactic sources should provide an upper limit to f_4. In both cases we find $f_4 \approx 0.6$. Allowing the disk to contribute to the scattering will require an even smaller f_4.

The estimate for A_1 in the previous section assumed $f_4 = 0$. Figure 5 also shows the estimate of A_1 obtained for $f_4 = 0.25$, with PSR B0611+22 and 0629+109 included in the fitting. Because of the additional scattering contributed by the arm, the estimates of A_1 are smaller, $A_1 \lesssim 15$ kpc for a sech^2 dependence and $A_1 \lesssim 22$ kpc for a truncated disk. The likelihood ratio between the sech^2 and truncated disk again favors the sech^2 disk by a factor of less than two.

In the following we reconsider our limit on A_1 while allowing the disk to flare and warp. Rather than conduct a search over the range $0 \leq f_4 \lesssim 0.6$, we shall evaluate the likelihood function at a fiducial value. Comparing the magnitudes of the likelihood functions for $f_4 = 0$ and $f_4 = 0.6$, the value $f_4 = 0$ is favored by more than an order of magnitude. We adopt $f_4 = 0.25$. With this value of f_4, the Perseus arm contributes an SM $\sim 6.25 \times 10^{-4}$ kpc m$^{-20/3}$, equivalent to a 1 GHz scattering diameter of 1.5 mas. Figure 5 indicates how a different choice for f_4 would affect the maximum likelihood value of A_1.

3.4.3. The Outer Ionized Disk

In addition to A_1 we shall be fitting for $h_{1,\rm out}$ and $F_{1,\rm out}$. Our initial ranges were centered approximately on the values in the TC93 model of 0.88 kpc and 0.4, respectively. Our initial range for $h_{1,\rm out}$ was $0.5\,{\rm kpc} \leq h_{1,\rm out} \leq 5\,{\rm kpc}$. The upper limit is comparable to the scale height for H I (Burton & te Lintel Hekkert 1986); the lower limit is approximately half the inner scale height, $h_{1,\rm in} = 0.88$ kpc. Further, the TC93-model value for the scale height of the material in the spiral arms is $h_{\rm a} = 0.3$ kpc. Values of $h_{1,\rm in} \lesssim 0.5$ kpc could indicate an underestimate of the scattering in the Perseus arm, i.e., f_4 is too low. Our initial range for $F_{1,\rm out}$ was $0 \leq F_{1,\rm out} \leq 2$. The lower limit describes a quiescent, i.e., non-scattering, outer disk. The fluctuation parameter for the spiral

arms is $F_{\rm a} = 6$ so fitted values of $F_{1,\rm out} \gtrsim 2$ could also indicate that the scattering contribution from the Perseus arm was underestimated.

Figure 6 compares the likelihoods for a sech^2 radial dependence *vs.* a truncated disk for an unwarped disk. The primary difference between these two models is that $A_1 \approx 22$ kpc for a truncated disk *vs.* $A_1 \approx 15$ kpc for the sech^2 disk. These differences are comparable to those found in the more simple model of Fig. 5.

The likelihood results favor $h_{1,\rm out} \approx 0.6$ kpc, as compared to value of 0.88 kpc for the inner Galaxy from the TC93 model. Above we identify an underestimate of the level of scattering in the Perseus arm as one means of producing $h_{1,\rm out} \lesssim h_{1,\rm in}$. We now identify three additional possibilities: (1) Misclassification of a source as extragalactic rather than Galactic; (2) Less scattering near the solar circle than predicted by the nominal TC93 model; or (3) A patchy distribution of scattering material.

If a source is classified as extragalactic, the model value of SM is calculated from an integral along the entire line of sight. If the source were instead classified as Galactic, the integral would extend out only to the source's estimated distance. Not only would a shorter path length result in a smaller SM and smaller predicted diameter, but the path would sample less of the material at large z. The scale height would be accordingly less constrained.

The diameter of the source 87GB 0600+2957 ($b = 4\fdg0$) is 1.5 mas. The predicted diameter of the source in the unwarped disk models described above is approximately 2.5 mas. The predicted diameter from the TC93 model is nearly 6 mas. If we repeat the above fitting, excluding 87GB 0600+2957 from the sample of sources, the maximum likelihood estimate of $h_{1,\rm out}$ nearly doubles, while the estimates of A_1 and $F_{1,\rm out}$ remain essentially unchanged. However, as we discuss in Paper I, we can find no compelling reason to classify this source as Galactic.

The second possibility is that the TC93 model may overestimate the level of scattering toward the anticenter. TC93 estimated the fluctuation parameter in the extended component to be $F_{1,\rm in} = 0.36^{+0.30}_{-0.10}$ and adopted a nominal value of $F_{1,\rm in} = 0.4$. We have repeated the analysis above with $F_{1,\rm in} = 0.3$. The likelihood results are essentially unchanged, as we might expect. This lower value of $F_{1,\rm in}$ is a reduction of only 25%, while the discrepancy between the observed and modelled diameters for 87GB 0600+2957 is nearly a factor of two. A lower value of $F_{1,\rm in}$ can reduce, but not eliminate, this discrepancy. We therefore conclude that the anticenter distribution of scattering material may contain holes or gaps—a source shining through one of these gaps would have an anomalously small scattering diameter.

Harrison & Lyne (1993) compared the velocities as determined by proper motions and interstellar scintillation pattern velocities for a number of high latitude pulsars. They concluded that the scale height of the scattering gas and of the ionized gas were markedly different: approximately 0.1 kpc for the former and 1 kpc for the latter. We assume that the scattering traces the distribution of ionized gas, however, our analysis considers only the scattering data. Regardless of the correct explanation for the small angular diameter of 87GB 0600+2957, we strongly disfavor

a scale height as small as 0.1 kpc and find the scale height to be 5–10 times larger.

Figure 7*a* shows the likelihood function for a warped disk, constructed using the observables from all 18 sources. The estimates of A_1 change only slightly from the unwarped disk. However, the estimates of $h_{1,\rm out}$ increase by more than a factor of five. Larger values of $h_{1,\rm out}$ are allowed primarily because of our coarse angular sampling. Scattering observables for sources near $\ell \approx 180^\circ$ are little affected by a warp in the disk. The warp is such that the maximum electron column density shifts to positive latitudes in the second quadrant and negative latitudes in the third. Examination of Fig. 3 shows that the warp generally increases the angular distance between sources and the midplane of the disk. Thus, larger scale heights are allowed, indeed required, in order to reproduce the observed source diameters.

In Fig. 7*b*, we assess the influence of the pulsars on the likelihood functions. The pulsars' contribution to the likelihood is constructed from the observed and modelled scintillation bandwidth, $\Delta\nu_{\rm d}$ and $\widehat{\Delta\nu_{\rm d}}$, respectively. In turn, $\widehat{\Delta\nu_{\rm d}}$ is a function of both $\widehat{\rm SM}$ and $\widehat{\rm DM}$, equation (14). The $\widehat{\rm DM}$ dependence occurs because $\widehat{\Delta\nu_{\rm d}}$ and the weighting function for $\widehat{\rm SM}$ both depend upon distance, which is estimated by integrating $n_{\rm e}\,ds$ until it equals the observed DM. In contrast, the scattering diameter for an extragalactic source is a function of only $\widehat{\rm SM}$, equation (2). Hence systematic errors in the model have a greater impact on the pulsars' contribution to the likelihood.

The regions of maximum likelihood in Figs. 7*a* and 7*b* overlap, though the allowed regions in Fig. 7*b* are somewhat larger. The larger regions are to be expected since fewer sources were used to constrain the model parameters. Comparing the left and right panels of Fig. 7, the most significant difference is in the maximum likelihood estimates for A_1 and $F_{1,\rm out}$. The m.l.e. for A_1 is smaller and the m.l.e. for $F_{1,\rm out}$ is larger when only extragalactic sources are used as compared to all sources. This difference is due primarily to the presence of 0629+109 in the sample. Its scattering diameter is large enough that considerable scattering, i.e., large $F_{1,\rm out}$, is needed. However, the smaller diameters of the other extragalactic sources then drive A_1 to smaller values in order that their scattering diameters not be overestimated. We have also repeated this analysis excluding 0629+109 from the sample. In this case the likelihood functions including and excluding the pulsars are nearly indistinguishable, indicating that the contribution of the extragalactic sources to the likelihood function dominates that of the pulsars.

3.5. Preferred Model

Our likelihood results favor the unwarped disk over the warped disk by a factor of 5–10. In both models, the $\rm sech^2$ and truncated radial dependences are nearly equally likely. We favor the truncated disk because its radial extent is in good agreement with the radial extent of sites of massive star formation, §4.1.2 (cf. Fig. 9).

The nominal set of parameters can be obtained largely by inspection of Fig. 6 and is summarized

in Table 3. We adopt $A_1 = 20$ kpc and $F_{1,\rm out} = 0.4$, the latter is slightly less than what Fig. 6 suggests, but is in good agreement with the value that TC93 derive for the inner Galaxy. Thus, the extended scattering component has a continuous fluctuation parameter through the onset of the warp. For the scale height $h_{1,\rm out}$ we adopt 1 kpc. This is larger than what Fig. 6 suggests, but, as we discuss above, the estimate of $h_{1,\rm out}$ is influenced by 87GB 0600+2957. A value of 1 kpc is intermediate between that value derived using 87GB 0600+2957 in the fitting and that value derived with 87GB 0600+2957 omitted from the fitting.

In Fig. 8 we show the contribution of the individual sources to the total likelihood of Fig. 6 (cf. also Fig. 5). This figure can be used to assess how well our model reproduces the observed scattering diameter. The fact that we have been able to limit A_1 has been due largely to the addition of two sources, 87GB 0600+2957 and 87GB 0621+1219 (Paper I). The remaining sources place either a lower limit on A_1 or do not constrain it very well at all. One source not shown on this figure is 0629+109. Its contribution to the likelihood is significantly less than the other sources. Since the line of sight to 0629+109 passes close to the H II region S273, this low likelihood could indicate either that our adopted value for f_4 is too small or that the assumption that spiral arms are smooth structures is beginning to break down.

This figure also demonstrates why using upper limits to the scattering diameters of all extragalactic sources in the anticenter would not be worthwhile, §3.2. Sources with upper limits to the scattering diameter significantly larger than the modelled value would produce on this plot flat lines coincident with the $\log p = 0$ abscissa.

4. Discussion and Conclusions

4.1. Free Electrons and Turbulence in the Outer Galaxy

Our likelihood results indicate that $A_1 \approx 15$ kpc if the fluctuating part of the electron density distribution exhibits a gradual decrease in the outer Galaxy or $A_1 \approx 20$ kpc if the H II disk is truncated. The apparent decrease in the rms $n_{\rm e}$ could result if sites of turbulence became less numerous while the mean $n_{\rm e}$ remained constant or it could result from decreases in the mean $n_{\rm e}$ itself. In this section we assess the extent to which our inferred value for A_1 can distinguish between these possibilities.

To discuss variations in the electron density, we recast equation (4) in terms of the H I density and ionization and integrate over a path length D,

$$\mathrm{SM} = \int_0^D C_{\rm u} F f X_{\rm i}^2 n_{\rm H}^2 \, ds. \tag{15}$$

In this form, it is clear that there are three means by which the amount of scattering in the outer Galaxy could be limited:

1. $n_{\rm H}$—It is well known that the distribution of H I decreases at large Galactocentric radii (Burton 1992). Outer Galaxy scattering could be limited because there is simply not enough gas to be ionized and produce scattering.

2. $fX_{\rm i}^2$—This factor is the product of the fractional ionization, $X_{\rm i}$, and the volume filling factor, f, of the ionized gas. If the number density of ionization sources, e.g., H II regions and supernovae, decreases faster than does $n_{\rm H}$, the scattering would be limited by a lack of ionized gas, even though there would be sufficient amounts of neutral gas. We treat the product $fX_{\rm i}^2$ rather than f and $X_{\rm i}$ separately because our measurements cannot distinguish between the two. Changes in f can be balanced by changes in $X_{\rm i}^2$ so as to keep the product constant.

3. F—This factor is a measure of the level of turbulence. Since the rate of star formation does fall off toward the outer Galaxy, unless alternate or additional sources of ionization are present in the outer Galaxy, e.g., the intergalactic ionizing flux, the scattering could be limited by a lack of turbulent energy input into the medium rather than the ionization.

Our motivation for assuming that SM is separable in this manner is to consider ionization and energy input mechanisms from sources not generally thought to be operative in the inner Galaxy. We consider each of these factors in turn.

4.1.1. Hydrogen Distribution

Outside the solar circle atomic hydrogen dominates molecular hydrogen (Gordon & Burton 1976) and we take $n_{\rm H} = n_{\rm H\,I}$. Comparison of the emission measure (EM $= \int n_{\rm e}^2\, ds$) and DM toward high-latitude pulsars suggest $f \gtrsim 0.1$ and $X_{\rm i} \approx 1$ (Reynolds 1977). Because we are assuming the strength of scattering in the outer Galaxy is dominated by the decrease in the H I density, we take f, $X_{\rm i}$, and F to be constant as a function of R.

We estimate the quantity $\int n_{\rm H\,I}^2\, ds$ toward the anticenter using the mass models of Dehnen & Binney (1997). We are required to use a model to estimate this quantity because the self-opacity of H I toward the anticenter means that the H I column density is not an observable (Burton & te Lintel Hekkert 1986).

Our estimate is $\int n_{\rm H\,I}^2\, ds \approx 2.3$ cm^{-6} kpc. Assuming that $F = 0.4$, the resulting SM is $\log_{10}({\rm SM}) = -0.8$. This SM produces a 1 GHz scattering diameter of 40 mas, approximately 2–5 times larger than what we observe. We conclude that the distribution of electron density turbulence must decrease more rapidly with Galactocentric distance than the distribution of hydrogen. This decrease may be due to an overall decrease in ionized gas or to a diminution of turbulence in the ionized gas.

4.1.2. Sources of Ionization: Stellar vs. Intergalactic

Interior to $R \approx 25$ kpc, the H I surface density is greater than 10^{19} cm^{-2} (Burton 1992; Dehnen & Binney 1997) and the disk is optically thick to the intergalactic ionizing flux. Consequently, $fX_{\rm i}^2$ should increase with R as the H I surface density and the disk's optical depth decrease. Patchiness in the outer Galaxy H I distribution would also increase $fX_{\rm i}^2$.

As the previous section showed, if $fX_{\rm i}^2 \approx 0.1$ and is constant as a function of R, the H I distribution overpredicts the scattering diameters. Allowing $fX_{\rm i}^2$ to increase with R would increase the size of this discrepancy. Further, the scale length of the scattering is smaller than the Galactocentric distance at which the disk becomes optically thin, indicating that the intergalactic ionizing flux does not play a significant role in the scattering in the outer Galaxy.

We favor star formation in the outer Galaxy as the more likely source of ionization. Wouterloot et al. (1990) showed that the distribution of molecular clouds with embedded massive star formation terminates at 20 kpc. This truncated distribution has an extent comparable to what our likelihood functions imply for the radial extent of scattering. The limited radial extent of the molecular clouds is also the reason we favor the truncated disk model to describe the radial dependence of scattering. Figure 9 illustrates schematically the spatially coincident distributions of molecular clouds and turbulent gas in the outer Galaxy.

4.1.3. Sources of Turbulence: Stellar vs. Galactic

The factoring of the scattering measure into separate ionization and turbulent contributions, equation (15), ignores possible correlations between these factors: Many of the same sources responsible for the ionization of the gas can also serve to produce turbulence, e.g., H II regions and supernovae. We utilize this factoring in order to consider an alternate source of turbulence not associated with massive star formation. We conclude that turbulence is in fact associated with star formation.

The orbits of the Magellanic clouds cause them to cross the midplane of the disk. As these and other satellite galaxies cross the disk, they generate mixing layers and wakes. The eddy turnover time, which is related to the energy dissipation rate, is $t \sim l_0/u$ (Tennekes & Lumley 1972) where l_0 is the outer scale of the turbulence and u is a characteristic velocity. For $l_0 \sim 100$ pc (Rickett 1990; Spangler 1991; and references within) and $u \sim 100$ km s^{-1}, $t \sim 10^6$ yr. Since the orbital period of a typical satellite galaxy is of order 10^9 yr, the passage of a satellite galaxy through the outer disk will provide only a transitory source of turbulence.

The distribution of molecular clouds with embedded massive star formation extends to 20 kpc (Wouterloot et al. 1990), comparable to the extent of the extended ionized component. The stars embedded in these molecular clouds have spectral types of early B (Wouterloot, Brand, & Henkel 1988). These stars are probably sufficiently powerful to produce turbulence: The pulsar

B0611+22 exhibits strong interstellar scintillation and the line of sight to it passes near several late O and early B stars (Weisberg et al. 1980).

4.2. Comparison with External Galaxies

Diffuse ionized gas in external galaxies has been detected in Hα emission (Rand 1996 and references within). This diffuse gas is presumably the equivalent of the Galaxy's warm ionized medium (Kulkarni & Heiles 1987). Spangler & Reynolds (1990) showed that the scattering diameters for extragalactic sources are correlated with Hα emission, suggesting that the same (warm ionized) gas responsible for the Hα emission is also responsible for the scattering. In this section we compare the radial extent of the Galaxy as inferred in our likelihood analysis with that determined for other galaxies.

Table 4 presents a subset of Hα measurements extracted from the literature. We restrict the list to those galaxies for which the published observations include images large enough that radial extents can be estimated reliably. The last entry in Table 4 is our estimate, based on the likelihood results, for the radial extent of the Galaxy as it would appear to an external observer. We have obtained this estimate in the following manner. The (1σ) sensitivities for the Hα observations are typically $\delta(\mathrm{EM}) \approx 3$ cm^{-6} pc. We integrated $n_\mathrm{e}^2\, ds$ to produce the modelled EM, $\widehat{\mathrm{EM}}$, along a line of sight appropriate for an external observer seeing the Galaxy edge on, i.e., along the path parallel to the x-axis (the discussion following eqn. [5] describes the coordinate system). Trial and error was sufficient to determine that, for a truncated disk, $\widehat{\mathrm{EM}} \approx \delta(\mathrm{EM})$ at $R \approx A_1/2$. The radial extent of the Galaxy is comparable to the radial extent of these other galaxies.

A measure of the star formation rate of the galaxy is provided by L_FIR/D_{25}^2, the far-infrared luminosity within the optical isophotal diameter at 25$^\mathrm{th}$ magnitude. This is an imperfect measure of the star formation rate, however, as low-mass stars heating "cirrus" clouds can contribute to the far infrared luminosity (Rand 1996) and the optical and infrared luminosities may have different extents.

Although the star formation rate, as measured by L_FIR/D_{25}^2, is a good predictor of the amount of extraplanar gas (Rand 1996), it is not well correlated with the radial extent of Hα. For instance, the radial extent of NGC 4217 is only 25% (4 kpc) smaller than that of UGC 10288 even though the star formation rate is at least a factor of three higher in UGC 10288; NGC 5746 has a radial extent larger than that of the Galaxy even though its star formation rate is an order of magnitude less than the Galaxy's. More likely, the star formation rate is determined by a quantity like the H I or H_2 surface density.

Further support for our proposal that our measurements trace the extent of the turbulent ionized disk is found by comparing the Hα emission in external galaxies (Rand 1996, Figs. 1–9) with the molecular cloud distribution in the outer Galaxy (Wouterloot et al. 1990, Fig. 4). The Hα emission is concentrated toward the galaxies' centers with a gradient to large radial distances.

Near the edge of the Hα disk, the emission becomes patchy. The molecular cloud distribution in the outer Galaxy has a similar appearance—it display a strong Galactocentric gradient and, for $R \approx 15$–20 kpc, the distribution is patchy.

High latitude structure in the extended component could influence our estimates for the various model parameters, in particular $h_{1,\rm out}$, §3.4.3. The morphology of the extraplanar diffuse gas in external galaxies shows considerable variety: NGC 891 shows diffuse gas up to 4 kpc off the plane with many vertical filaments (Rand, Kulkarni, & Hester 1992); UGC 10288 shows vertical filaments but no diffuse gas (Rand 1996); NGC 4278 shows patchy emission (Rand 1996); and NGC 4565 shows little halo diffuse gas (Rand et al. 1992). Hα observations of the diffuse gas in the solar neighborhood show filamentary structure (Ogden & Reynolds 1985) and the vertical morphology of the extended component could be quite complex.

4.3. Conclusions

We have modified the outer Galaxy portion of the Taylor-Cordes model for the global distribution of ionized gas. Our modifications are motivated by the observed warping and flaring of the H I, H_2, and stellar constituents of the outer Galaxy. The data available to constrain the model consist of 18 sources, 9 extragalactic sources from a survey we conducted (Paper I) and 7 pulsars and 2 extragalactic source extracted from the literature (Table 2). We used a likelihood analysis to constrain the model parameters. The two most important parameters are the radial scale length of the ionized disk, A_1 and the strength of scattering in the Perseus arm. The adopted model parameters are summarized in Table 3.

The scattering in the Perseus arm is, at most, 60% of the level seen in the inner Galaxy spiral arms. This upper limit assumes that all of the scattering for sources toward $\ell \sim 180^\circ$ is due to the Perseus arm. Our analysis favors a level of scattering less than this upper limit. We adopt a value 25% that in the inner Galaxy; the equivalent scattering diameter is 1.5 mas at 1 GHz.

We considered two different radial dependences for the electron density, a smooth decrease of the electron density with Galactocentric distance, equation (6), and a truncated distribution, equation (7). The current data cannot distinguish between these two forms. The radial scale length for the ionized disk is $A_1 \approx 15$–20 kpc, comparable to the extent that TC93 adopted with fewer anticenter measurements. We favor the truncated disk because the radial extent inferred for sites of massive star formation also appears truncated at approximately 20 kpc, as indicated schematically in Fig. 9. Hα observations of external galaxies show that they have radial extents comparable to that which we infer for the Galaxy.

Our analysis favors an unwarped, non-flaring disk with a scale height of 1 kpc, though this may reflect the non-uniform and coarse coverage of the anticenter provided by the available data.

The observed scattering diameter of one extragalactic source (87GB 0600+2957) is a factor

of two smaller than the modelled scattering diameter, suggesting the possibilities of holes in the scattering material. The Hα emission in the outer portions of the disks of these external galaxies also appears patchy, similar to the distribution of molecular clouds in the outer Galaxy. A patchy distribution of massive star formation sites would allow the possibility of holes in the scattering material.

We conclude that scattering in the outer Galaxy traces star formation, as it does in the inner Galaxy. The intergalactic ionizing flux and turbulence generated by satellite galaxies passing through the disk contribute little to the scattering. However, the ionized disk of the Galaxy could extend to much larger radii ($R \gtrsim 100$ kpc), comparable to that inferred from Lyα absorption systems (e.g., Charlton et al. 1993), if the extreme outer disk is quiescent and contributes little scattering.

We thank P. Goldsmith, D. Chernoff, and T. Herter for helpful conversations. We thank the referee for a suggestion that led to Fig. 8. This research has made use of the Simbad database, operated at the CDS, Strasbourg, France. This research was supported by NASA GRO grants NAG 5-2436 and NAG 5-3515 and NSF grant AST-9528394.

REFERENCES

Bland-Hawthorn, J. 1997, Publ. Astron. Soc. Aust., 14, 1

Bland-Hawthorn, J., Freeman, K. C., & Quinn, P. J. 1997, ApJ, in press

Bregman, J. N. 1980, ApJ, 236, 577

Burke, B. F. 1957, AJ, 62, 90

Burton, W. B. 1992, in The Galactic Interstellar Medium, eds. D. Pfenniger & P. Bartholdi (Berlin: Springer-Verlag) p. 1

Burton, W. B. & te Lintel Hekkert, P. 1986, A&AS, 65, 427

Carney, B. W. & Seitzer, P. 1993, AJ, 105, 2127

Charlton, J. C., Salpeter, E. E., & Hogan, C. J. 1993, ApJ, 402, 493

Corbelli, E. & Salpeter, E. E. 1993, ApJ, 419, 104

Corbelli, E., Schneider, S. E., & Salpeter, E. E. 1989, AJ, 97, 390

Cordes, J. M. & Lazio, T. J. 1991, ApJ, 376, 123

Cordes, J. M., Weisberg, J. M., Frail, D. A., Spangler, S. R., & Ryan, M. 1991, Nature, 354, 121

Cordes, J. M. 1986, ApJ, 311, 183

Dehnen, W. & Binney, J. 1997, MNRAS, submitted

Dennison, B., Thomas, M., Booth, R. S., Brown, R. L., Broderick, J. J., & Condon, J. J. 1984, A&A, 135, 199

Djorgovski, S. & Sosin, C. 1989, ApJ, 341, L13

Fey, A. L., Spangler, S. R., & Cordes, J. M. 1991, ApJ, 372, 132

Fey, A. L., Spangler, S. R., & Mutel, R. L. 1989, ApJ, 337, 730

Frail, D. A. & Weisberg, J. M. 1990, AJ, 100, 743

Freudenreich, H. T., et al. 1994, ApJ, 429, L69

Gordon, M. A. & Burton, W. B. 1976, ApJ, 208, 346

Gwinn, C. R., Bartel, N., & Cordes, J. M. 1993, ApJ, 410, 673

Harrison, P. A. & Lyne, A. G. 1993, MNRAS, 265, 778

Houck, J. C. & Bregman, J. N. 1990, ApJ, 352, 506

Isaacman, R. 1977, Nature, 268, 317

Isaacman, R. & Rankin, J. M. 1977, ApJ, 214, 214

Kahn, J. D. 1991, in IAU Symposium 144, The Interstellar Disk-Halo Connection in Galaxies, ed. H. Bloeman (Dordrecht: Kluwer), p. 1

Kellermann, K. I. & Owen, F. N. 1988, in Galactic and Extragalactic Radio Astronomy, eds. G. L. Verschuur & K. I. Kellermann (Berlin: Springer-Verlag) p. 563

Kerr, F. J. 1957, AJ, 62, 93

Kulkarni, S. R. & Heiles, C. 1987, in Interstellar Processes, eds. D. J. Hollenbach & H. A. Thronson, Jr. (Dordrecht: Reidel) p. 87

Lazio, T. J. W. & Cordes, J. M. 1997, ApJ, submitted (Paper I)

Ogden, P. M. & Reynolds, R. J. 1985, ApJ, 290, 238

Oort, J. H., Kerr, F. J., & Westerhout, G. 1958, MNRAS, 118, 379

Rand, R. J. 1996, ApJ, 462, 712

Rand, R. J., Kulkarni, S. R., & Hester, J. J. 1992, ApJ, 396, 97

Rand, R. J., Kulkarni, S. R., & Hester, J. J. 1990, ApJ, 352, L1

Rendong, N., Schilizzi, R. T., Fanti C., & Fanti R. 1991, A&A, 252, 513

Resch, G. M. 1974, Ph. D. Thesis, Florida State Univ.

Reynolds, R. J. 1983, ApJ, 268, 698

Reynolds, R. J. 1977, ApJ, 216, 433

Rickett, B. J. 1990, ARA&A, 28, 561

Savage, B. D., Sembach, K. R., & Lu, L. 1995, ApJ, 449, 145

Shapiro, P. R. & Field, G. B. 1976, ApJ, 205, 762

Sodroski, T. J., Dwek, E., Hauser, M. G., & Kerr, F. J. 1987, ApJ, 322, 101

Spangler, S. R. 1991, ApJ, 376, 540

Spangler, S. R., Mutel, R. L., Benson, J. M., & Cordes, J. M. 1986, ApJ, 301, 312

Spitzer, L., Jr. 1990, ARA&A, 28, 71

Sunyaev, R. 1969, Astrophys. Lett., 3, 33

Taylor, J. H. & Cordes, J. M. 1993, ApJ, 411, 674 (TC93)

Taylor, J. H., Manchester, R. N., & Lyne, A. G. 1993, ApJS, 88, 529

Tennekes, H. & Lumley, J. L. 1972, A First Course in Turbulence (Cambridge: MIT)

Vandenberg, N. R. 1976, ApJ, 209, 578

van Gorkom, J. 1991, in Atoms, Ions, and Molecules: New Results in Spectral Line Astrophysics, eds. A. D. Haschick & P. T. .P. Ho (San Francisco: ASP) p. 1

Veilleux, S., Cecil, G., & Bland-Hawthorn, J. 1995, ApJ, 445, 152

Weisberg, J. M., Rankin, J., & Boriakoff, V. 1980, A&A, 88, 84

Westerhout, G. 1957, Bull. Astron. Inst. Netherlands, 13, 201

Wilkinson, P. N., Readhead, A. C. S., Anderson, B., & Purcell, G. H. 1979, ApJ, 232, 365

Wouterloot, J. G. A., Brand, J., Burton, W. B., & Kwee, K. K. 1990, A&A, 230, 21

Wouterloot, J. G. A. & Brand, J. 1989, A&AS, 80, 149

Zepka, A., Cordes, J. M., Wasserman, I., & Lundgren, S. C. 1996, ApJ, 456, 305

Fig. 1.— The angular broadening for an extragalactic source observed toward the anticenter as a function of A_1, the Galactocentric scale length in the Taylor-Cordes model. The curves are labelled by the observation frequency in GHz. The nominal resolutions of the Very Long Baseline Array and an array containing the HALCA VLBI satellite are shown as dotted lines.

Fig. 2.— The functional forms for the radial dependence of $n_{\rm e}$ in the outer Galaxy. The solid line shows the radial dependence of the H I volume density (Gordon & Burton 1976; Burton 1992); the long-dash line shows the sech^2 dependence of equation (6); and the short-dash line shows the truncated disk of equation (7). All quantities are normalized to pass through unity at $R = R_\odot$.

Fig. 3.— The angular distribution of low-latitude anticenter sources with measured scattering observables. The plotted symbol is proportional to the logarithm of the 1 GHz scattering diameter. Circles show scattering diameters from this program, squares show scattering diameters for extragalactic sources reported in the literature, and stars show the diameters of pulsars. Except for the Crab, $(\ell, b) = (184^\circ, -5^\circ)$, the pulsar diameters are inferred from the pulsar's scintillation bandwidth and require an estimate of the pulsar's distance. The contour increments are 1 mas with the highest contour being 7 mas. *Top*: The contours show the scattering diameters as predicted by the Taylor-Cordes model. *Bottom*: The contours show the scattering diameters as predicted by a warped, non-flaring model for the disk. The onset of the warp is at $R = 10.5$ kpc and the warped disk is inclined by $\Psi = 20^\circ$ to the inner Galaxy's midplane, viz. Fig. 4.

Fig. 4.— The geometry of the tilted ring model for the outer ionized disk. A source with Galactic coordinates (ℓ, b) has a latitude b' relative to the tilted ring's midplane. The scale height of the disk exterior to $R = 10.5$ kpc is also shown.

Fig. 5.— Likelihood estimates of A_1 for an unwarped, non-flaring disk. The solid line shows the likelihood results for a disk with a radial sech^2 dependence of equation (6), the dashed line for a truncated disk of equation (7). *Top*: The likelihood function if the Perseus spiral arm is ignored. *Bottom*: The likelihood function if the Perseus spiral arm has a strength 25% that of the inner Galaxy spiral arms.

Fig. 6.— Likelihood function contours for pairs of parameters that include the disk scale length, A_1, scale height, $h_{1,\rm out}$, and fluctuation parameter, $F_{1,\rm out}$. The disk is unwarped. Contours show the 67%, 90%, and 99% confidence regions. Crosses mark the location of the maximum likelihood. *Left panels*: sech^2 radial dependence for the disk, equation (6); and *Right panels*: truncated disk, equation (7). The sharp edges in these likelihood functions are real and result from fluctuations in the likelihood function caused by the small number of data. They do not reflect the grid resolution in the grid searches.

Fig. 7.— As for Fig. 6. The model disk is warped with $\Psi = 20^\circ$ and $\ell_0' = 170^\circ$ and has a sech^2 dependence. *Left*: Likelihood function constructed using all data; and *Right*: Likelihood function constructed using only extragalactic sources.

Fig. 8.— The contribution of the individual sources to the likelihood function for the truncated disk model in Fig. 6 (cf. also Fig. 5). We have held all parameters fixed at their maximum likelihood estimated value (viz. Table 3), except A_1. Sources whose individual likelihoods fall below 0.1 for any value of A_1 are identified explicitly. The log likelihood for the source 0629+109 is sufficiently low that it is not shown.

Fig. 9.— A schematic of scattering in the outer Galaxy. Small, dark regions are molecular clouds from the CO survey of Wouterloot & Brand (1989). Cross-hatched regions represent turbulent gas, responsible for the scattering, potentially surrounding these clouds, resulting from embedded star formation. This figure illustrates how the scattering gas could follow the distribution of molecular gas.

Table 1. Scattering Diameters at 1 GHz from the Survey of Lazio & Cordes (1997)

Name	ℓ (°)	b (°)	θ_s (mas)
87GB 0433+4706	157.3	−0.0	<48
87GB 0451+4309	162.5	−0.1	< 5.1
87GB 0512+2627	178.5	−6.6	< 6.8
87GB 0537+3059	177.9	0.2	< 3.7
87GB 0547+3044	178.9	1.8	< 6.1
87GB 0558+2325	186.5	0.3	3.7±0.8
87GB 0600+2957	180.9	4.0	1.5±0.4
87GB 0621+1219	198.8	−0.4	2.8±0.1
87GB 0622+1153	199.4	−0.3	<18

Table 2. Scattering Measurements from the Literature

Name	ℓ (°)	b (°)	$\Delta\nu_d$ (MHz)	θ_s (mas)	D (kpc)	Ref.
PSR B0301+19	161.14	−33.27	9.55±2.4	0.29±0.097	0.94	1
PSR B0320+39	152.18	−14.33	2.291±0.77	0.46±0.15	1.47	1
PSR B0450+55	152.62	7.54	9.55±2.4	0.29±0.097	0.78	1
PSR B0525+21	183.86	−6.89	0.62±0.2	0.72±0.24	2.27	1
PSR B0531+21	184.60	−5.80	···	0.50±0.05	2.0	4
PSR B0540+23	184.36	−3.31	0.11±0.03	1.4 ±0.47	3.53	1
PSR B0611+22	188.79	2.39	0.04±0.01	2.0 ±0.67	4.72	1
PSR B0626+24	188.82	6.22	0.08±0.02	1.4 ±0.47	4.69	1
PSR B0656+14	201.11	8.25	8.51±2.1	0.34±0.11	0.76	1
PSR B0823+26	196.96	31.74	9.55±2.4	0.29±0.097	0.37	1

Table 2—Continued

Name	ℓ (°)	b (°)	$\Delta\nu_{\rm d}$ (MHz)	$\theta_{\rm s}$ (mas)	D (kpc)	Ref.
PSR B1112+50	154.41	60.36	19.50±6.4	0.26±0.087	0.54	1
0503+467	161.00	3.70	···	< 4	···	2
0629+109	201.50	0.50	···	25 ±1.4	···	3

Note. — All quantities have been scaled to 1 GHz. The scattering angle for the pulsars depends upon both the scintillation bandwidth and adopted distance, $\theta_{\rm s} = 0.85\,{\rm mas}/\sqrt{D_{\rm kpc}\Delta\nu_{\rm d}}$.

References. — (1) Cordes (1986); (2) Spangler et al. (1986); (3) Dennison et al. (1984); (4) Gwinn et al. (1993)

Table 3. Preferred Model Parameters

Model Parameter	Adopted Value
radial form	truncated disk
n_1[a](cm^{-3})	0.0188
$h_{1,\rm in}$[a](kpc)	0.88
$F_{1,\rm in}$	0.4
f_4	0.25
A_1 (kpc)	20
$h_{1,\rm out}$ (kpc)	1
$F_{1,\rm out}$	0.4
Ψ (°)	0

[a]This parameter was not varied in our likelihood analysis; its value is taken from the Taylor-Cordes model.

Table 4. Radial Extent of Ionized Disks for External Galaxies

Name	R (kpc)	$L_{\rm FIR}/D_{25}^2$ $10^{40}\,{\rm erg\,s^{-1}\,kpc^{-2}}$	δ(EM) (pc cm^{-6})	Ref.
NGC 891	15	2.2	6.5	1
NGC 3079	11	8.9	10	3
NGC 4013	9	2.6	2.5	4
NGC 4217	12	<0.12	3.2	4
NGC 4302	10	<2.3	2.1	4
NGC 4565	17	0.3	2.3	2
NGC 4631	14	1.8	3.2	2
NGC 4762	6	<0.15	2.4	4
NGC 5023	4	<0.09	2.3	4
NGC 5746	26	0.2	3.7	4

Table 4—Continued

Name	R (kpc)	$L_{\rm FIR}/D_{25}^2$ $10^{40}\,{\rm erg\,s^{-1}\,kpc^{-2}}$	δ(EM) (pc cm^{-6})	Ref.
NGC 5907	22	0.8	3.2	4
UGC 4278	8	<0.04	2.7	4
UGC 10288	16	0.4	4.4	4
Galaxy	10	3.0	···	5

References. — (1) Rand, Kulkarni, & Hester (1990); (2) Rand, Kulkarni, & Hester (1992); (3) Veilleux, Cecil, & Bland-Hawthorn (1995); (4) Rand (1996); (5) this work

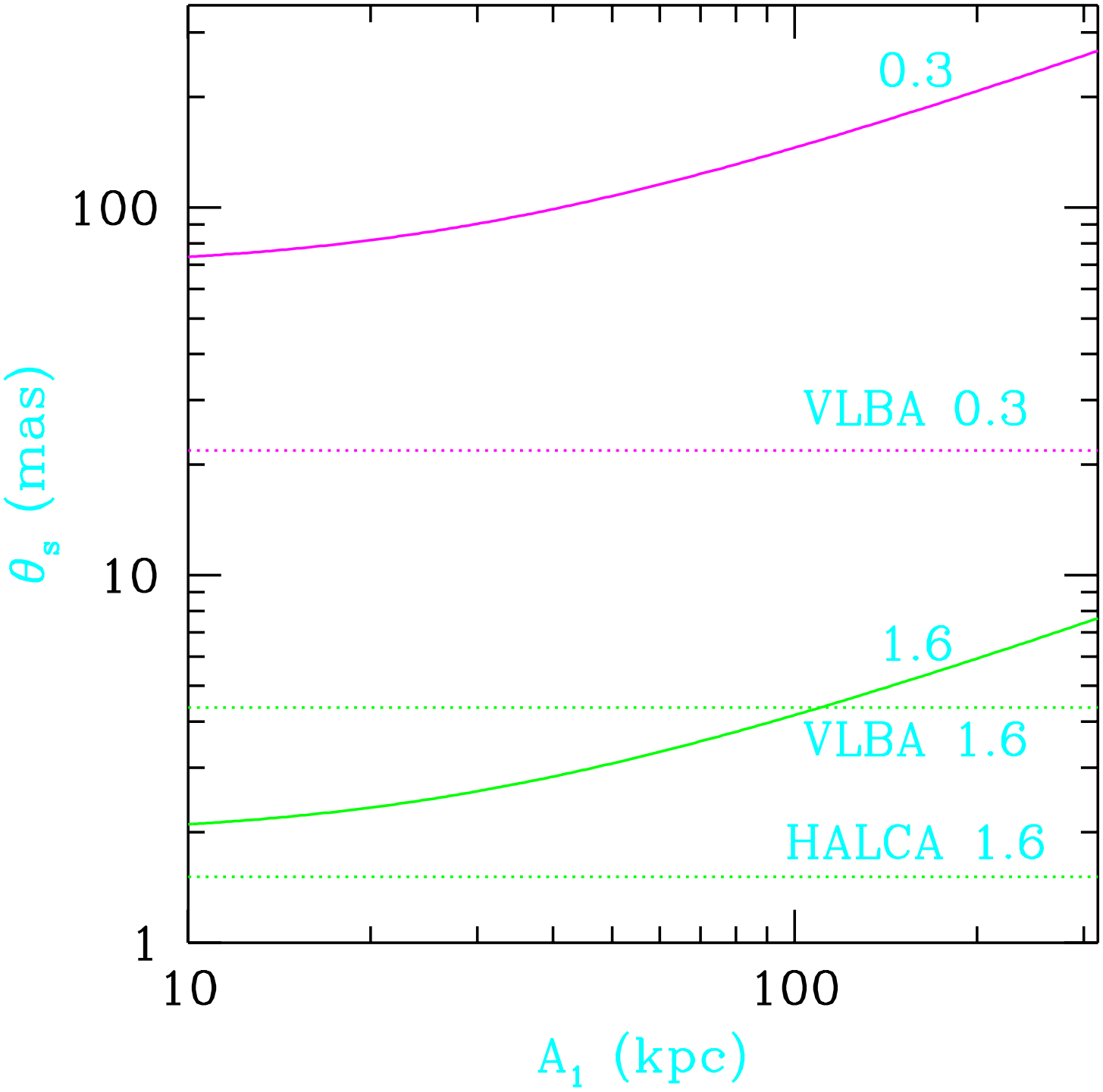
0.3
100
VLBA 0.3
θ_s (mas)
10
1.6
VLBA 1.6
HALCA 1.6
1
10
100
A_1 (kpc)

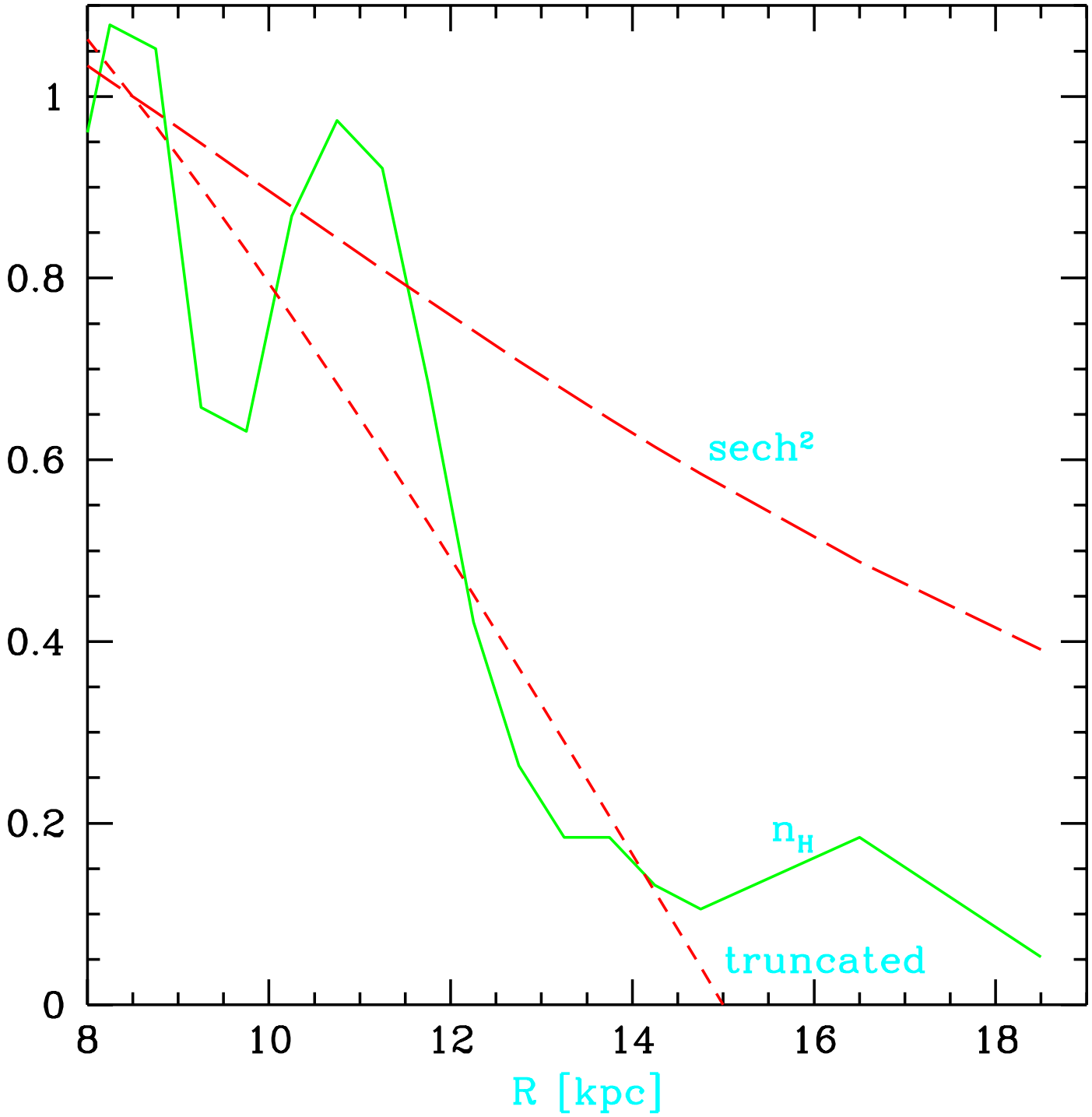
1
0.8
0.6
0.4
0.2
0
8
10
12
14
16
18
R [kpc]
sech²
n_H
truncated

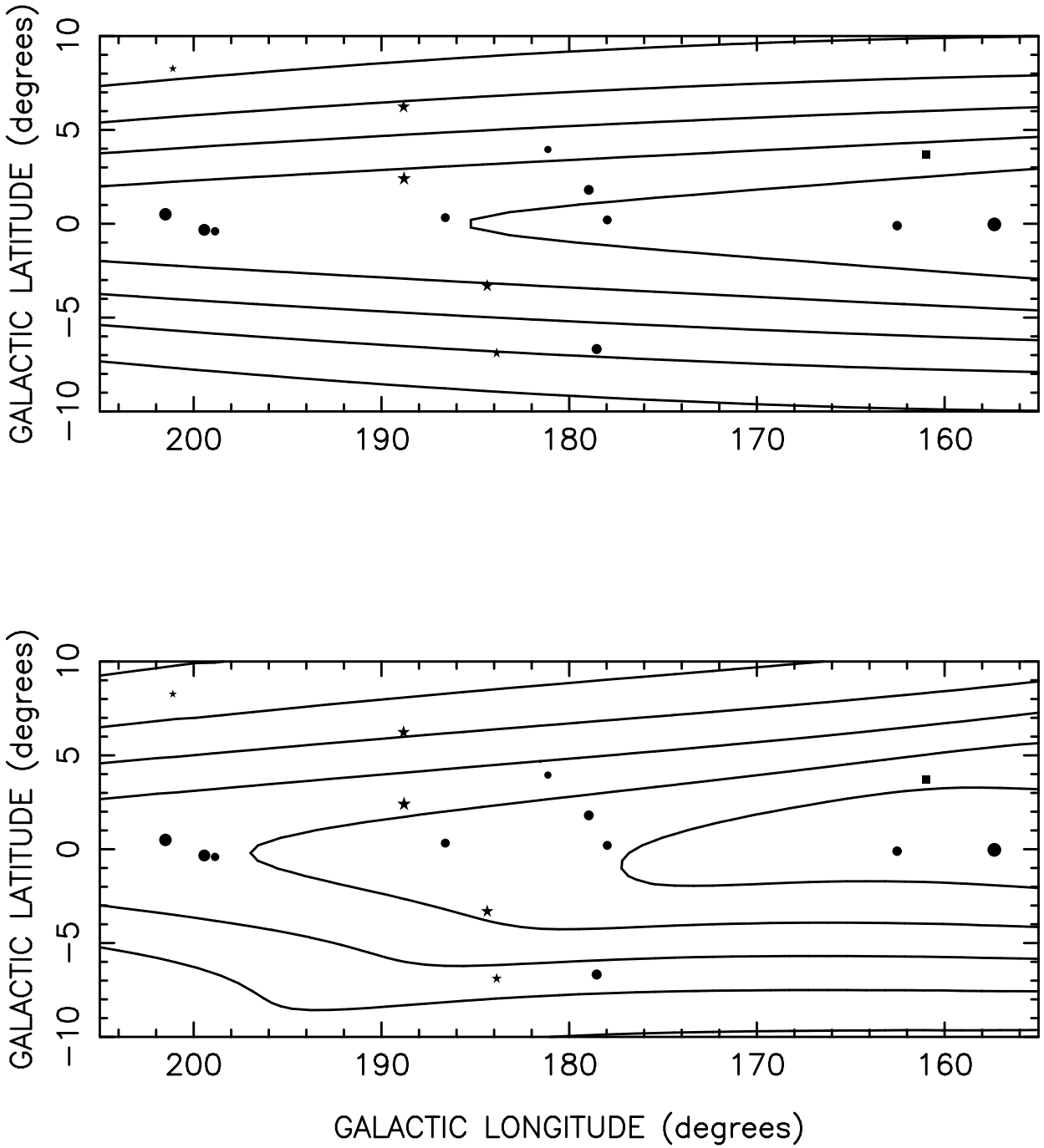
GALACTIC LATITUDE (degrees)
10
5
0
−5
−10
200
190
180
170
160
GALACTIC LONGITUDE (degrees)

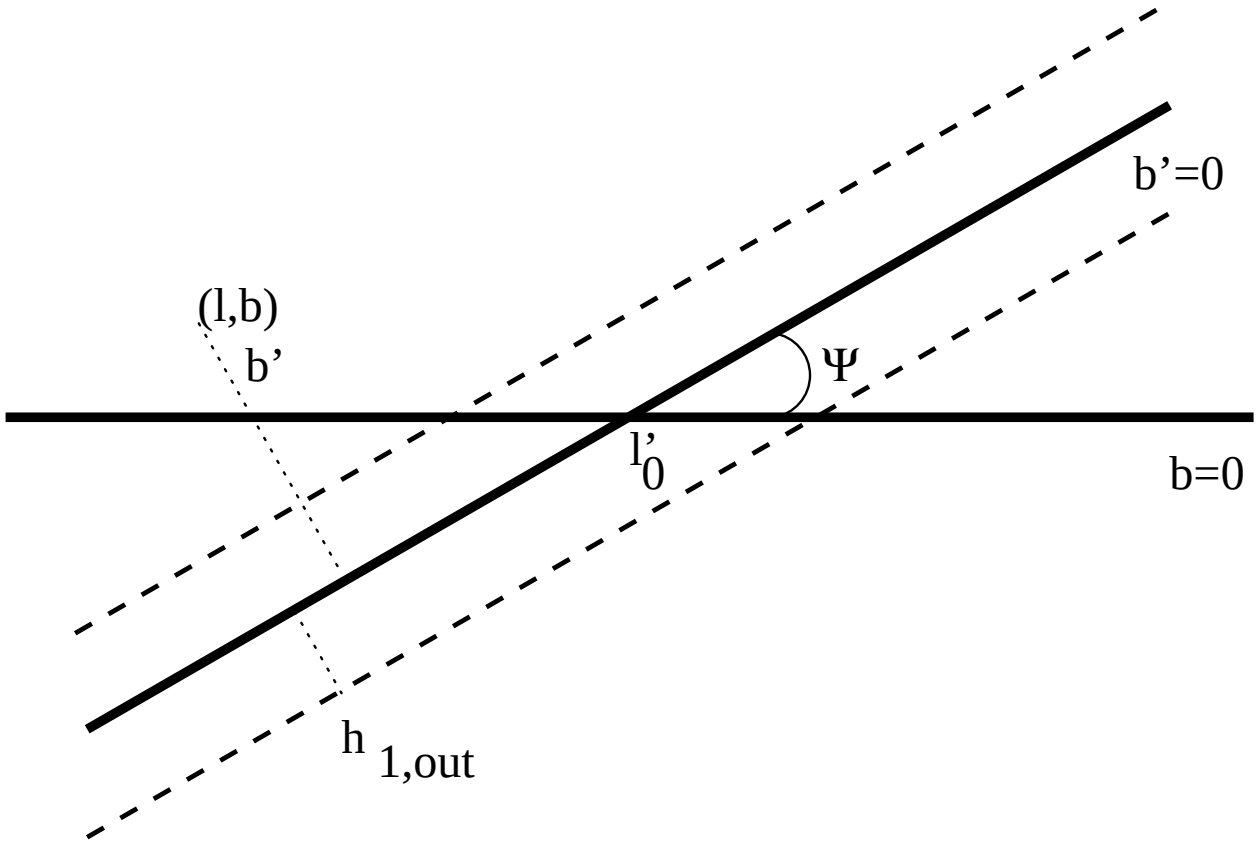
b'=0
(l,b)
b'
Ψ
l'0
b=0
h 1,out

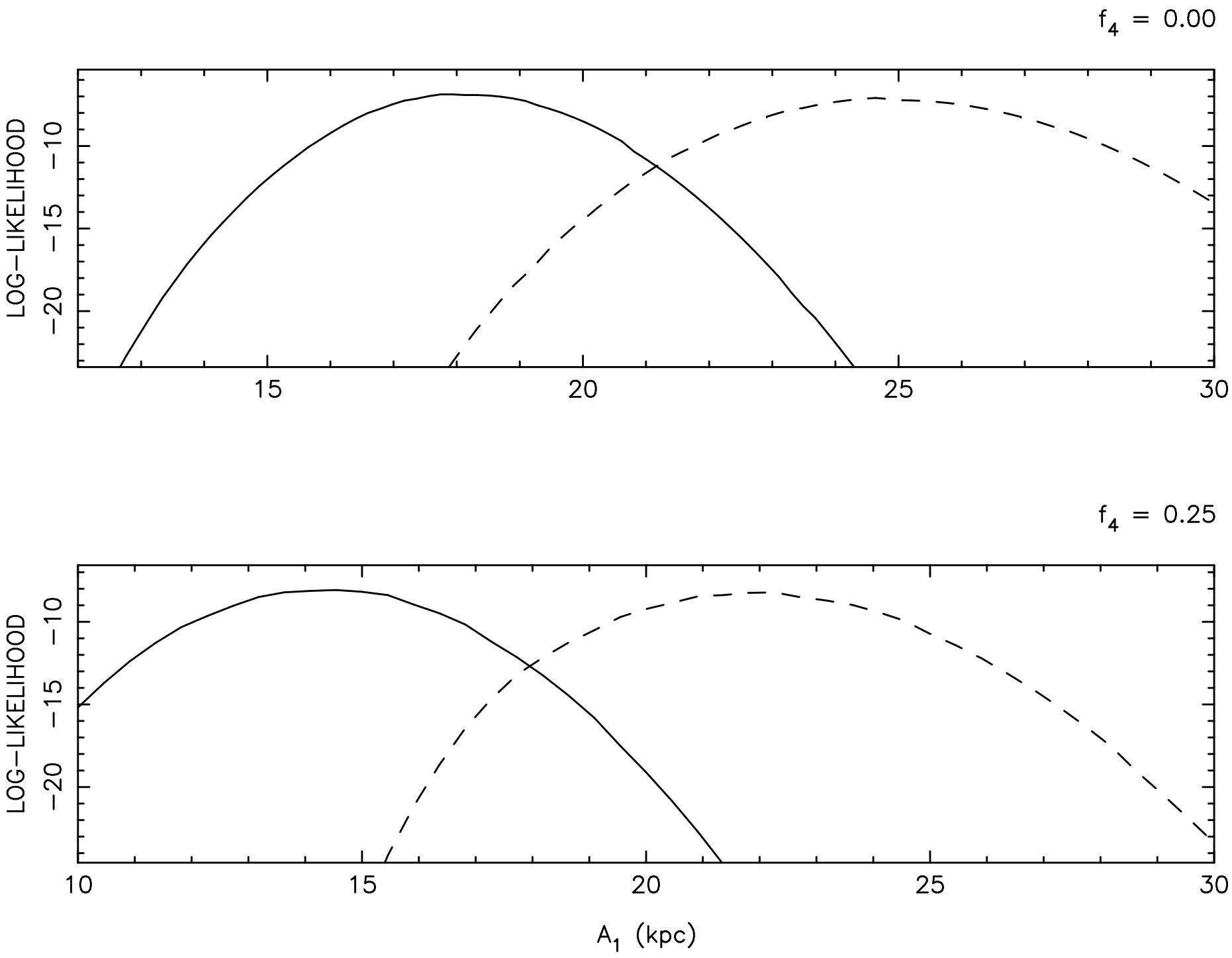
f_4 = 0.00
LOG−LIKELIHOOD
−10
−15
−20
15
20
25
30
f_4 = 0.25
LOG−LIKELIHOOD
−10
−15
−20
10
15
20
25
30
A_1 (kpc)

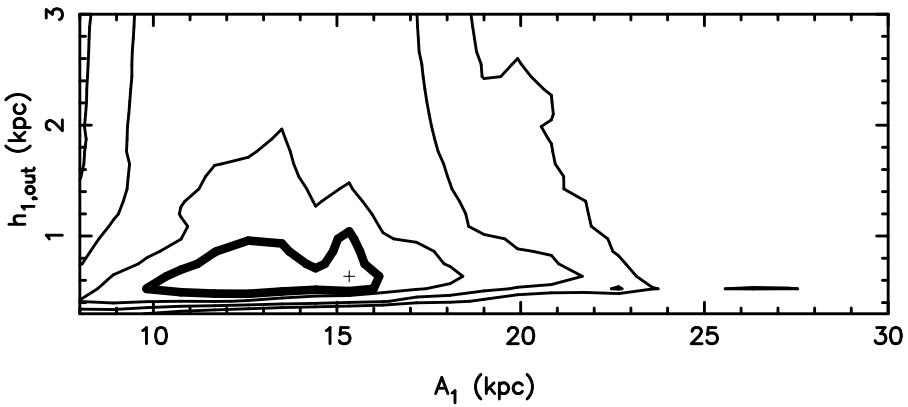
$h_{1,out}$ (kpc)
A_1 (kpc)

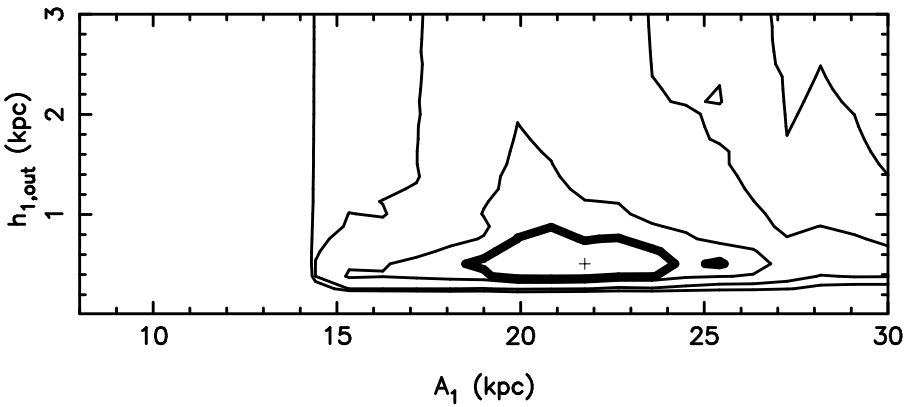
$h_{1,out}$ (kpc)
A_1 (kpc)

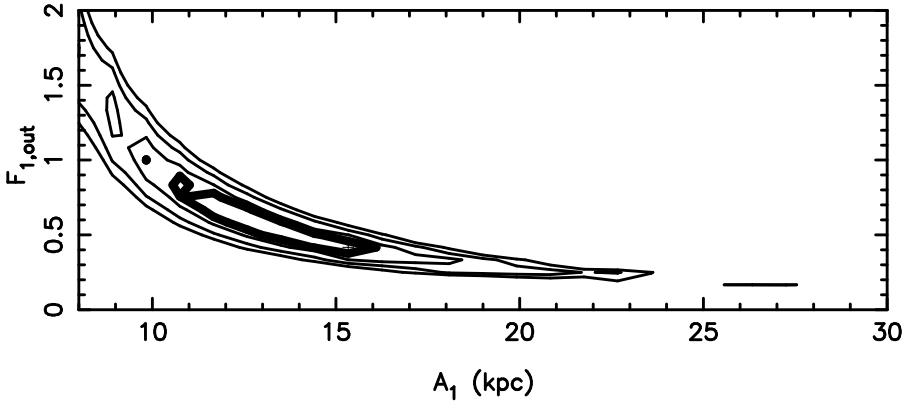
$F_{1,out}$
A_1 (kpc)

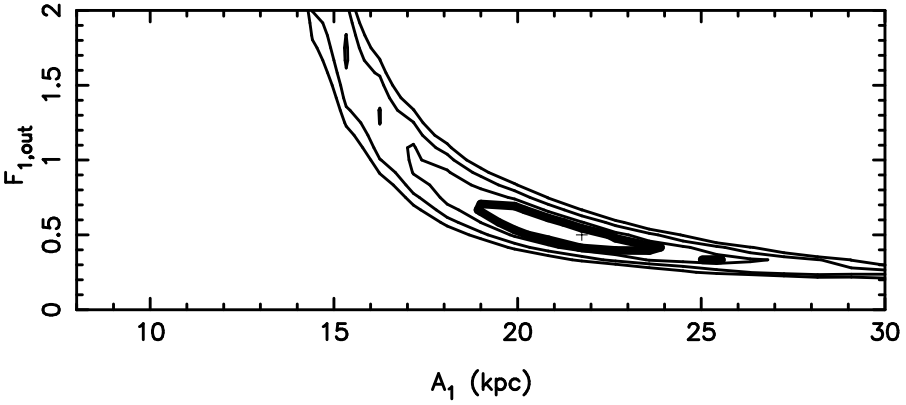
$F_{1,out}$
A_1 (kpc)

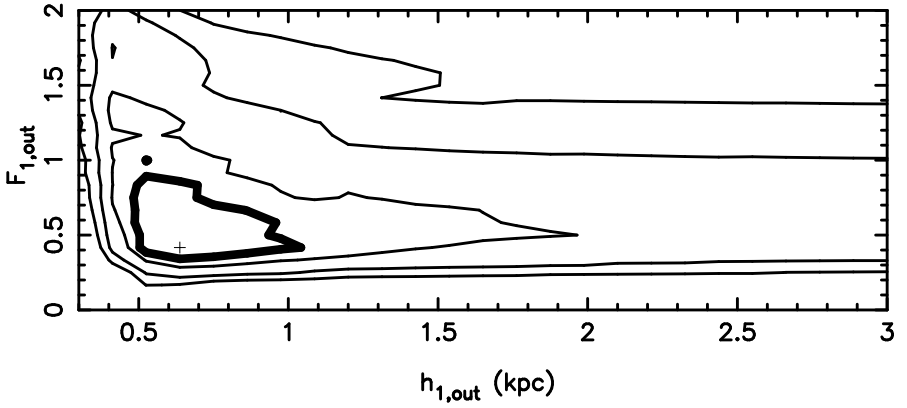
$F_{1,out}$
$h_{1,out}$ (kpc)

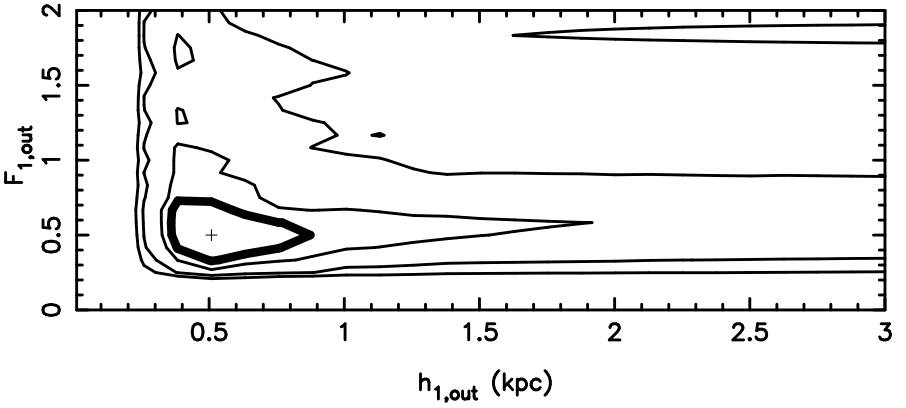
$F_{1,out}$
$h_{1,out}$ (kpc)

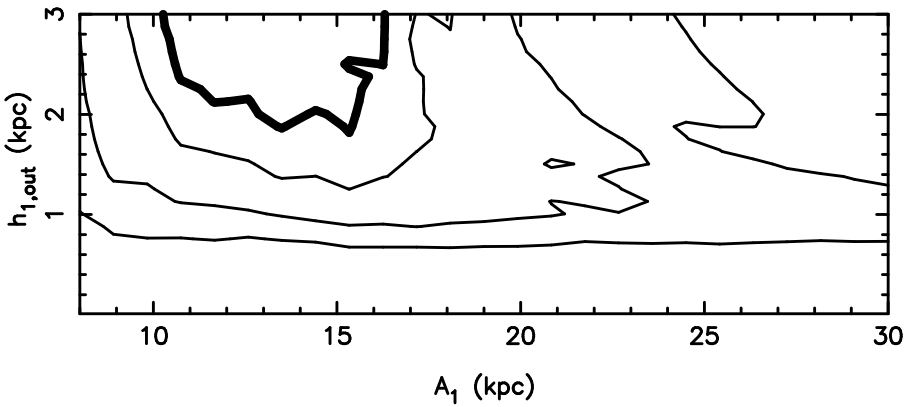
h1,out (kpc)
A1 (kpc)

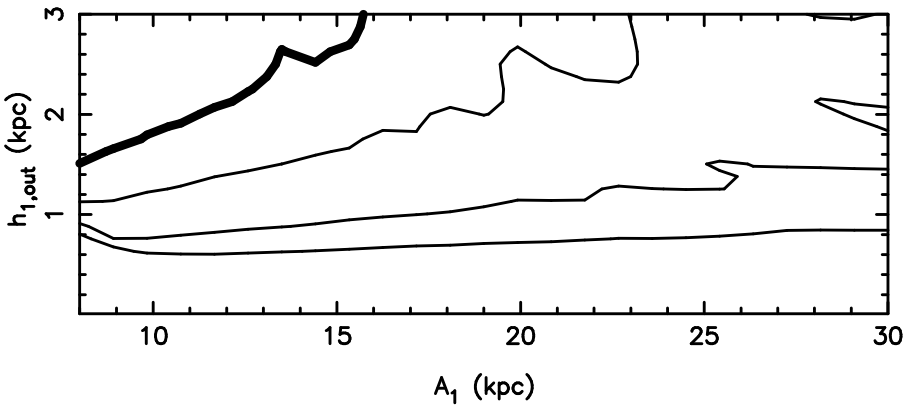
h1,out (kpc)
A1 (kpc)

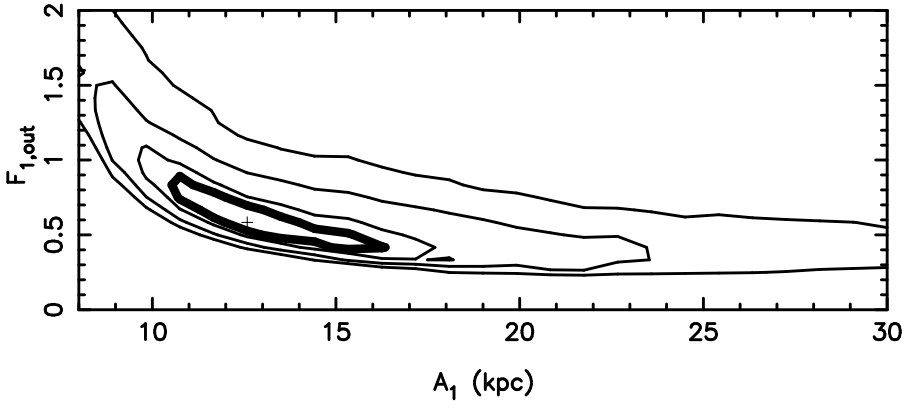
F1,out
A1 (kpc)

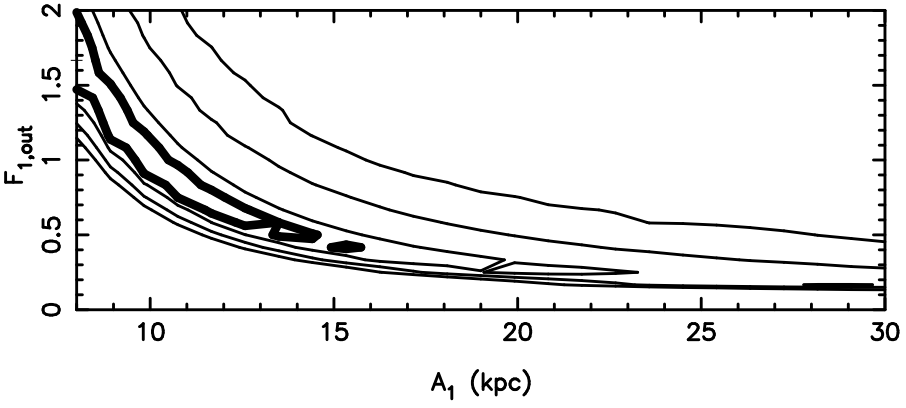
F1,out
A1 (kpc)

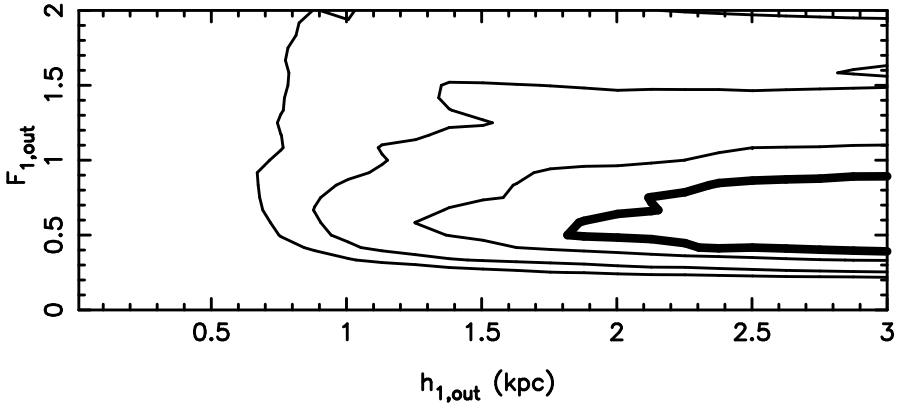
F1,out
h1,out (kpc)

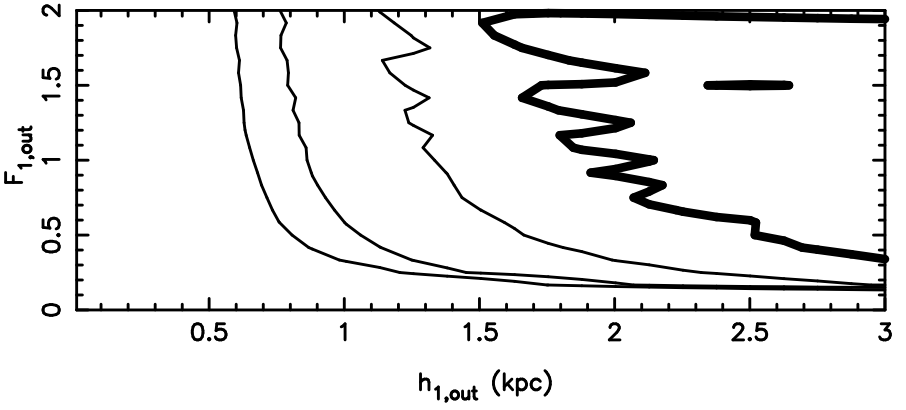
F1,out
h1,out (kpc)

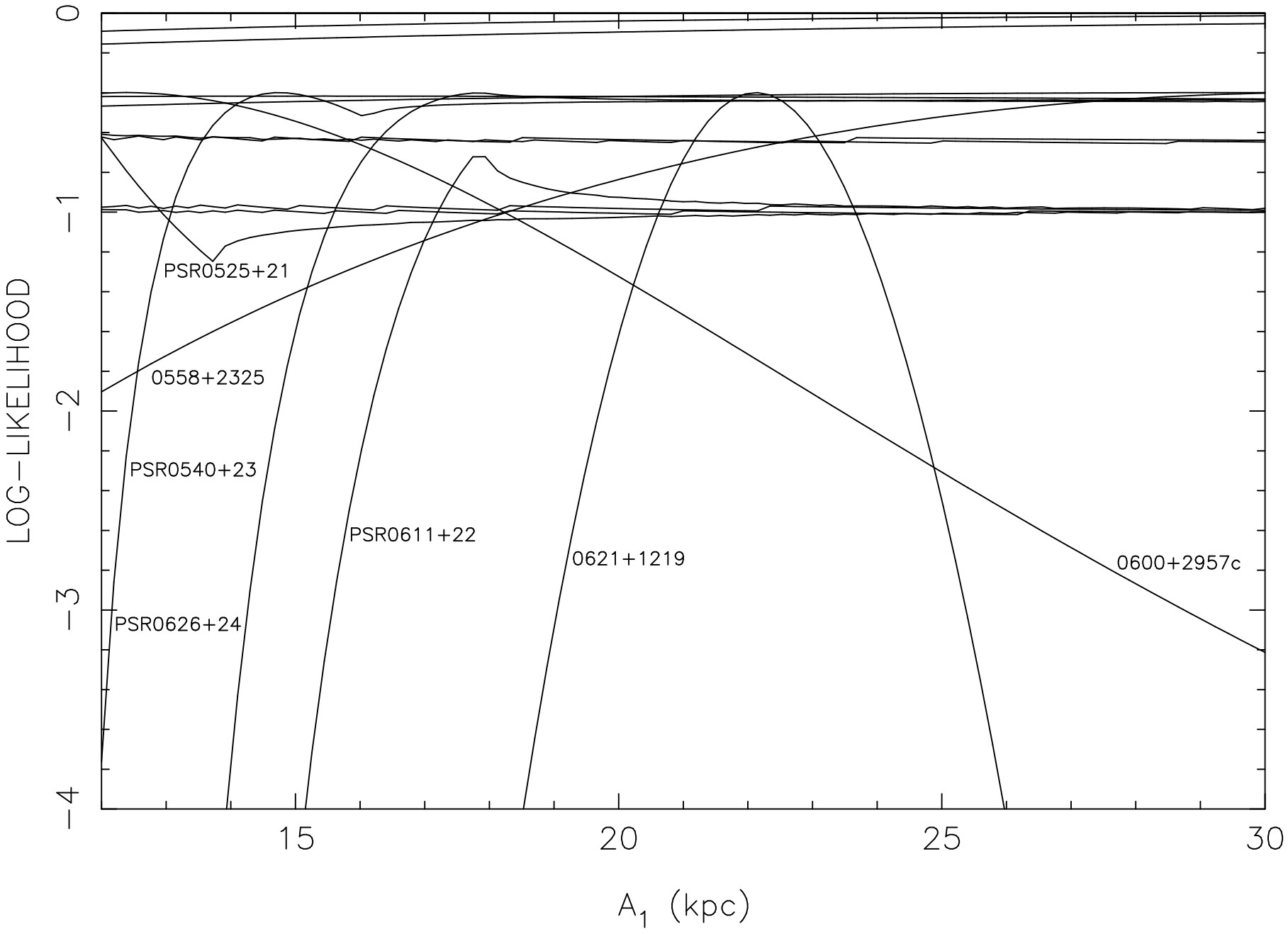
LOG−LIKELIHOOD
0
−1
−2
−3
−4
15
20
25
30
A1 (kpc)
PSR0525+21
0558+2325
PSR0540+23
PSR0611+22
0621+1219
0600+2957c
PSR0626+24

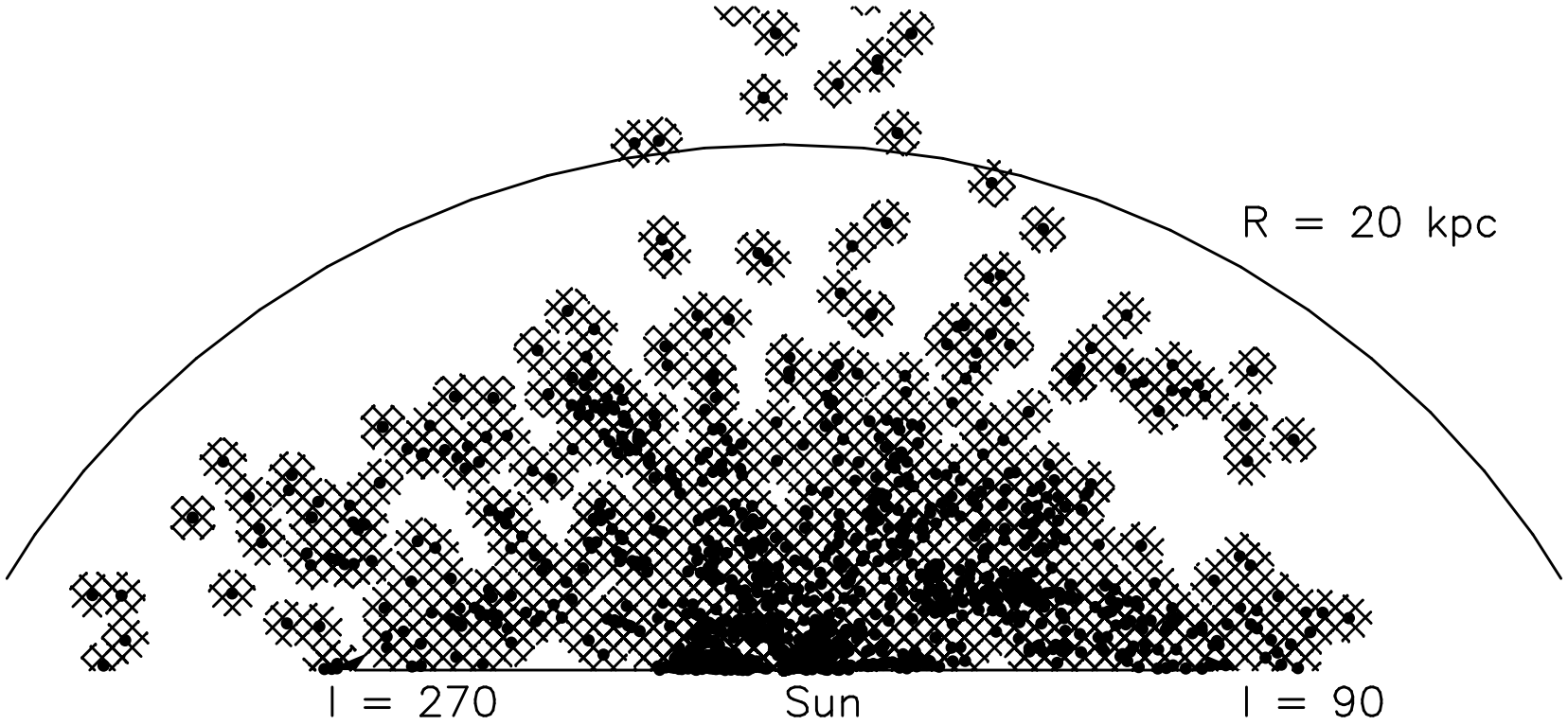
R = 20 kpc
l = 270
Sun
l = 90